# New Insights into the Allosteric Mechanism of Human Hemoglobin from Molecular Dynamics Simulations

Liliane Mouawad, David Perahia, Charles H. Robert, and Christophe Guilbert
Laboratoire de Modélisation et Ingénierie des Protéines, Institut de Biochimie et de Biophysique Moléculaire et Cellulaire, Centre National de la Recherche Scientifique, Unité Mixte de Recherche 8619, Université Paris-Sud, 91405 Orsay cedex, France

ABSTRACT It is still difficult to obtain a precise structural description of the transition between the deoxy T-state and oxy R-state conformations of human hemoglobin, despite a large number of experimental studies. We used molecular dynamics with the Path Exploration with Distance Constraints (PEDC) method to provide new insights into the allosteric mechanism at the atomic level, by simulating the T-to-R transition. The T-state molecule in the absence of ligands was seen to have a natural propensity for dimer rotation, which nevertheless would be hampered by steric hindrance in the "joint" region. The binding of a ligand to the $\alpha$ subunit would prevent such hindrance due to the coupling between this region and the $\alpha$ proximal histidine, and thus facilitate completion of the dimer rotation. Near the end of this quaternary transition, the "switch" region adopts the R conformation, resulting in a shift of the $\beta$ proximal histidine. This leads to a sliding of the $\beta$-heme, the effect of which is to open the $\beta$-heme's distal side, increasing the accessibility of the Fe atom and thereby the affinity of the protein. Our simulations are globally consistent with the Perutz strereochemical mechanism.

## INTRODUCTION

Human hemoglobin (Hb A) is an allosteric oxygen-binding protein that adopts two distinct conformations: the low-affinity deoxygenated T state and the high-affinity fully liganded R state. A mechanism for the transition from one conformation to the other upon ligand binding has been proposed by Perutz (1970), Perutz et al. (1998), and Baldwin and Chothia (1979). In this mechanism, the binding of a ligand to one subunit modifies the position of the proximal histidine (F8) with respect to the heme, inducing a movement of the FG segment (the segment that connects helices F and G), which forms a part of the $\alpha1\beta2$ interface. The adjustment of this interface causes dimer rotation and modifies the network of hydrogen bonds and salt bridges at the $\alpha1\beta2$ interface. This decreases the strain on the proximal histidine of the facing subunit and modifies the ligand accessibility to the heme iron atom in the $\beta$ subunit by "opening" its distal side. These structural modifications result in an increase of the protein affinity. The Perutz mechanism provides the best framework for understanding much of the experimental results on oxygen binding, although several points remain unclear. One is the role played by the $\alpha1\beta1$ interface. This interface is not referred to in this mechanism, but several experimental results (Levy et al., 1992; Tsai et al., 1999, 2000; Mihailescu and Russu, 2001) suggest that its role is not negligible. There is also an aspect of the proposed mechanism that is difficult to explain, in that the binding of ligand to the $\alpha$ subunits is supposed to induce the quaternary transition, as is seen experimentally in solution (Ogawa and Shulman, 1972; Fujii et al., 1993; Kiger et al., 1993; Unzai et al., 1998), whereas the conformational changes seen in these subunits are minimal as compared to the $\beta$ chains.

A tremendous number of experiments have been carried out to study the allosteric transition and to try to trap intermediate structures along this path. Most solution studies suggest that, under physiological conditions, Hb passes through a quaternary R-like intermediate state (Ogawa and Shulman, 1972; Murray et al., 1988; Eaton et al., 1991; Henry et al., 1997). However, crystal structures of partly liganded Hb have indicated a quaternary T-like structure (Luisi and Shibayama, 1989; Luisi et al., 1990; Waller and Liddington, 1990; Liddington et al., 1992; Bruno et al., 2000), but this may reflect the experimental constraints (such as the presence of allosteric effectors, low temperature, etc.). It also might be noted that even a fully liganded Hb has been crystallized in the T structure under certain conditions (Paoli et al., 1996). Moreover, a mutant carbonmonoxyHb (Hb Ypsilanti, $\beta$99Asp→Tyr) (Smith et al., 1991), and a wild-type carbonmonoxyHb (R2) that was crystallized at low salt concentration (Silva et al., 1992) were first described as being in an intermediate state between T and R. However, computer simulations, based on docking and distance calculations, suggested that it is instead the R form that is intermediate between T and R2 (Srinivasan and Rose, 1994), or between T and Hb Y (Janin and Wodak, 1993).

Only a few molecular simulations have been carried out for Hb because of its large size, which makes them very time-consuming. Thus, some simulations have been done

*Submitted September 19, 2001, and accepted for publication December 26, 2001.*

This paper is dedicated to the memory of Max F. Perutz.

Address reprint requests to Liliane Mouawad, Laboratoire de Modélisation et Ingénierie des Protéines, Institut de Biochimie et de Biophysique Moléculaire et Cellulaire, CNRS UMR8619, Bâtiment 430, Université Paris-Sud, 91405 Orsay cedex, France. Tel.: +33-01-69-15-63-20; Fax: +33-01-69-85-37-15; E-mail: liliane.mouawad@mip.u-psud.fr.

Christophe Guilbert's present address is Dept. of Pharmaceutical Chemistry, Univ. of California, 513 Parnassus Ave, San Francisco, CA 94143-0446.



0006-3495/02/06/3224/22 $2.00

with only a part of the protein, such as the $\alpha$ subunit (Gelin et al., 1983), the $\alpha1\beta2$ interface (Gao et al., 1989), or the $\alpha1\beta1$ dimer (Ramadas and Rifkind, 1999), or by using a rigid-body docking approach (Janin and Wodak, 1985). However, in the last decade, increases in the power of computers have made it possible to study the entire protein (Shibayama et al., 1995b; Mouawad and Perahia, 1996; Kim et al., 2001). Still, to our knowledge, no simulation of the transition path of Hb by molecular dynamics (MD) has been published.

The problem with studying large-scale conformational transitions by traditional molecular dynamics is that, even in very long simulations, the transition will occur rarely, if at all. Different methods have been introduced to attack this problem. One approach involves generating an initial guess for a trajectory leading from the starting to the final conformation, and then optimizing this trajectory to obtain the best transition pathway (Elber and Karplus, 1987; Ulitsky and Elber, 1990; E1-Kettani and Durup, 1992; Fischer and Karplus, 1992; Olender and Elber, 1996; Ulitsky and Shalloway, 1997; Huo and Straub, 1997; Zaloj and Elber, 2000). This approach requires the generation of a large number of intermediate structures in the initial trajectory to properly sample the conformational space. The computational penalty associated with optimizing such a large number of intermediate structures simultaneously can be limiting for a large protein such as Hb. A second class of approaches is sequential, i.e., it involves inducing the transition in a single molecule simulation from one conformational state to the other (Harvey and Gabb, 1993; Schlitter et al., 1994; Guilbert et al., 1995; Csajka and Chandler, 1998; Zuckerman and Woolf, 1999; Geissler and Chandler, 2000). In most of these latter methods, the length of the simulation, or the number of the intermediate structures, is predetermined, which may constitute a difficulty for large proteins where some readjustments can be harder to attain than initially estimated.

We present here the first MD simulations of the T-to-R transition in human Hb. For this we used a combination of MD with the path exploration by distance constraint method (PEDC) (Guilbert et al., 1995). The value of this method is that it is sequential but without predetermination of the length of the simulation, and also that it gives the possibility of simulating a pathway by MD (i.e., not only by energy minimization) at ambient temperature in presence of the solvent. This method consists of the addition to the potential energy of a constraint term that forces the protein (in our case the deoxygenated T-state Hb A) to approach a reference conformation (here, the fully oxygenated R-state Hb A), by decreasing the mass-weighted root-mean-square (mrms) deviation between the two conformations by a series of displacements, each consisting of several picoseconds of MD (here $\sim$10 ps, see Methods). Two separate trajectories (TrajI and TrajII) of 200 ps each, corresponding to 16 intervals of displacement, were performed to bring deoxygenated hemoglobin from the T state to the R state.

The simulated pathways made it possible to predict the presence of transient events, especially at the $\alpha1\beta1$ interface, and resulted in a mechanism consistent with the Perutz stereochemical mechanism, but with a different chronology of events. This mechanism makes clearer the difference in roles played by the $\alpha$ and $\beta$ subunits in Hb affinity and cooperativity.

## METHODS

### Description of the method

The PEDC method (Guilbert et al., 1995), which we implemented in the CHARMM program (Brooks et al., 1983), involves the addition of three constraint terms to the potential energy usually used in MD simulations. The main constraint is the distance constraint potential, $V_{\text{dist}}$, which forces the system toward a given mrms deviation from a reference, whereas the other two terms, $V_{\text{trans}}$ and $V_{\text{rot}}$ prevent the system from satisfying the distance constraint by overall translation or rotation, respectively. The distance constraint potential $V_{\text{dist}}$ is harmonic,

$$V_{\text{dist}} = \frac{k_{\text{dist}}}{2}(d^{\text{R}} - d_{\text{J}}^{0})^2.$$

Here $k_{\text{dist}}$ is the force constant, $d^{\text{R}}$ the mrms between the system and the reference structure $R$, and $d_{\text{J}}^{0}$ the target mrms that the system must ideally reach in a discrete displacement phase $J$. To explore the transition pathway between the initial structure $I$ and the reference structure $R$, each displacement phase $J$ involves decreasing $d_{\text{J}}^{0}$ by a value $\Delta d$ and carrying out MD or energy minimization (EM) runs. Thus, step by step, the system reaches the reference structure by the least energetically costly path consistent with the constraints.

However, this harmonic potential, which is very satisfactory for EM, is less suitable for MD. Indeed, driving the system toward the reference structure requires a relatively large force constant for the constraint potential, which may restrain the normal fluctuations of the system. We therefore adopted a flat-bottomed-well potential. Thus, in this study, $V_{\text{dist}}$ was of the form (Fig. 1),

$$V_{\text{dist}} = \begin{cases} \tfrac{1}{2}k_{\text{dist}}(d^{\text{R}} - (d_{\text{J}}^{0} - \delta d))^2 & d^{\text{R}} < (d_{\text{J}}^{0} - \delta d) \\ 0 & (d_{\text{J}}^{0} - \delta d) \le d^{\text{R}} \le (d_{\text{J}}^{0} + \delta d), \\ \tfrac{1}{2}k_{\text{dist}}(d^{\text{R}} - (d_{\text{J}}^{0} + \delta d))^2 & d^{\text{R}} > (d_{\text{J}}^{0} + \delta d) \end{cases}$$

The width of the flat bottom of the well, $2\delta d$, was set at a value a little larger than the average rms fluctuations of hemoglobin at 300 K, i.e., $2\delta d$ = 0.8 Å. The force constant, which, in the case of a harmonic potential, must be small to prevent damping of the fluctuations, should, in the case of the flat-bottomed-well potential, be very large to confine the system to the well. We used $k_{\text{dist}} = 10^6$ kcal/mol/Å$^2$. Such a large value does not perturb the system when it is inside the desired well, but is nevertheless not suitable for displacement of the system from one well to another, because it will induce large forces. Hence, the displacement phase is divided into two parts: the driving phase, in which the force constant is increased gradually from 200 to $10^6$ kcal/mol/Å$^2$ (see the transition pathways in the Procedure) to move the system into the energy well, and the confinement phase, in which MD is carried out using the constraint ($V_{\text{dist}}$) described above, with a force constant equal to $10^6$ kcal/mol/Å$^2$, to keep the system within the well.

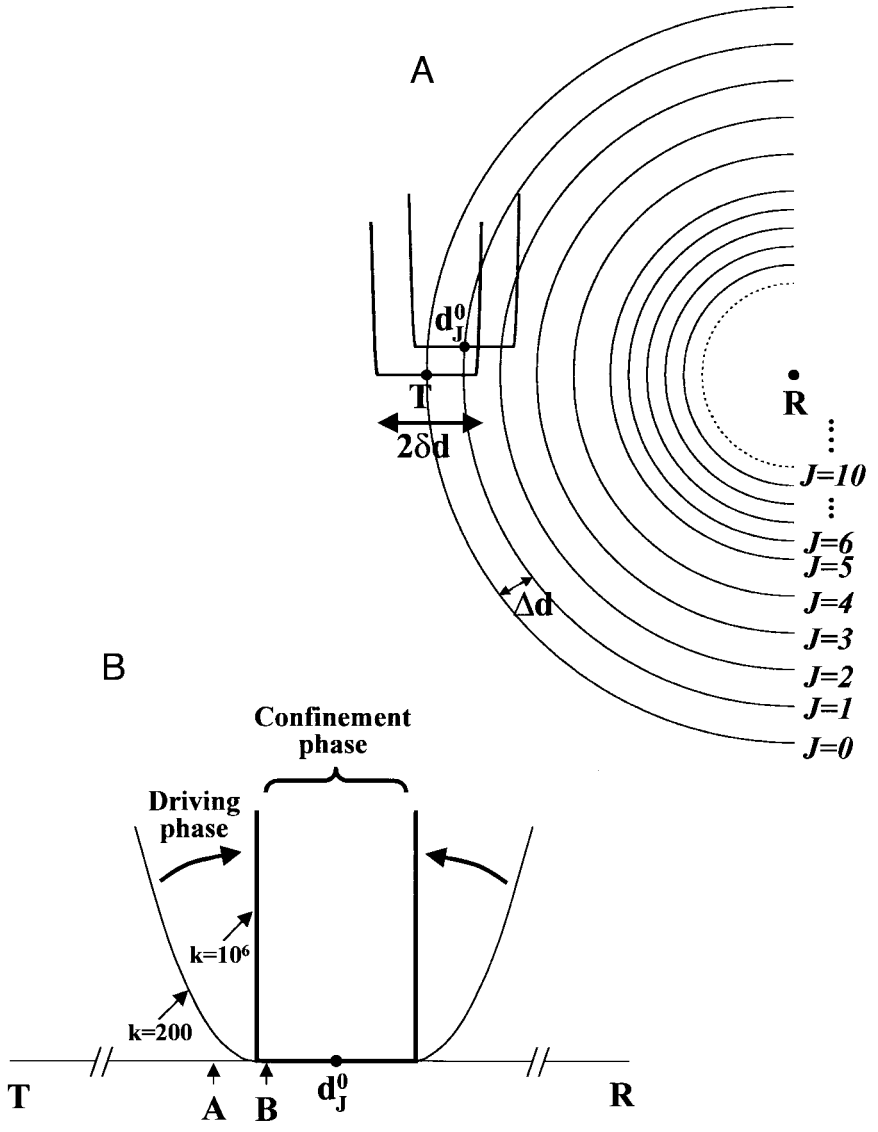


FIGURE 1 (*A*) Schematic representation of the spherical iso-mrms surfaces defined by the PEDC procedure with respect to the R structure. The PEDC constraint (i.e., the flat-bottomed-well potential) is shown centered at the starting T structure ($J = 0$, black) and at an intermediate mrms target $d_J^0$ (here $J = 1$, gray). The width of the well $2\delta d$ equalled 0.8 Å in our simulations, and the displacement step $\Delta d = 0.3$ Å until $J = 5$, at which point it was reduced to 0.15 Å. (*B*) The procedure for displacement from one interval to the next ($J - 1$ to $J$) consists of a driving phase, in which the force constant is increased gradually from 200 to $10^6$ kcal/mol/Å$^2$ (see text), to allow the structure to be brought smoothly into the next potential well (centered on $d_J^0$) for the confinement phase. At the end of interval $J - 1$, the structure may be either outside (**A**) or inside (**B**) the confinement region $J$ because of the overlap of the wells. In the second case (**B**), the energy of constraint during the driving phase will already be zero, as was seen at the beginning of TrajI.

## Procedure

This study was carried out on hemoglobin in a box of water with periodic boundary conditions.

### *The force field*

The force field parameters were set as follows: the QUANTA/CHARMm21 parameter set for extended atoms (with polar hydrogens explicitly represented) was used for amino acids and TIP3 water, and the all-hydrogens CHARMM22 parameter set was used for heme, to prevent artefactual distortions of this prosthetic group.

### *The water box*

It was important to choose the truncation functions for electrostatic and van der Waals energies that yielded a radial distribution function of water $g(r)$ that best fitted experimental data. Several MD trajectories of 10 ps each were calculated for boxes of water of different dimensions, with different combinations of truncation functions and cutoff distances. The combination that yielded the best radial distribution of water was the shift function for electrostatic energy with a cutoff distance of 11 Å and the switch function for the van der Waals energy with cuton and cutoff values of 10.5 and 11 Å, respectively. The water box considered was cubic, with the length of each side equal to the largest diameter of the protein in either state plus two times the cutoff distance. Thus, the length of the side of the box was 92 Å. Such dimensions were necessary to prevent direct interactions between the protein (or even the first layer of water) and its images, because movements of large amplitude were expected to be observed. This water box was constructed and equilibrated at 300 K. In all that follows, the MD was carried out in a microcanonical ensemble (constant volume and energy) with the Verlet algorithm (Verlet, 1967); the time step was equal to 1 fs with the use of the SHAKE algorithm (Ryckaert et al., 1977) applied to all covalent bonds involving hydrogen atoms. Because water molecules are considered explicitly, the value of the dielectric constant was set equal to 1.

### *The protein*

The structure of the deoxy T-state Hb A used in this study was derived from PDB (Bernstein et al., 1977) entry 2HHB (Fermi et al., 1984). A

rigorously symmetric mean structure was generated for both dimers to start the simulations, as described in Mouawad and Perahia (1996). In the oxy R state of Hb A, the PDB structure designated 1HHO (Shaanan, 1983) shows only one dimer, the other being obtained by symmetry. We point out that symmetry was not maintained artificially in the MD calculations and the structure was therefore free to evolve in a different way for each dimer. In both T and R structures the tautomeric forms of the histidines were assigned in a way that favored the formation of hydrogen bonds. None of them was protonated.

The potential energy of the protein was slightly minimized in vacuum, using the conjugate gradient algorithm of CHARMM, to eliminate unfavorable interactions due to crystal imprecision. In the first 300 steps, harmonic constraints (not to be confused with PEDC constraints) were applied to heavy atoms to allow smooth minimization without any abrupt deviations from the crystal structure. The harmonic force constant was decreased every 50 steps, taking the values of 250, 100, 50, 25, 10, and 5 kcal/mol/Å$^2$. We then carried out free minimization for 300 steps.

### *The protein in the water box*

Hemoglobin, along with the crystallographic water molecules, was immersed in the center of the water box. All water molecules that overlapped either protein or crystallographic water molecules (i.e., distance between heavy atoms less than 2.8 Å) were deleted, leaving a system of 66,723 atoms, 5,598 of which corresponded to the protein itself.

The protein's temperature was close to 0 K because its energy was minimized, whereas the temperature of the water was 300 K. To homogenize the system, the protein was fixed and the temperature of water was decreased to 0 K in 5 ps. The whole system was then heated to 300 K in 50-K intervals over 7 ps. This procedure was applied to both T and R structures. The oxygen ligands were kept in the heating phase for the R-state structure.

The resulting R structure was used as the reference $R$ in the PEDC method to compute the transition pathway. For comparison, two transition pathways were calculated; both used the same reference structure and started from the same minimized T structure but were heated with different Gaussian assignments of velocities. We refer here to these two trajectories as I and II.

### *The transition pathways*

The same procedure was applied for both trajectories. The system was equilibrated at 300 K for 10 ps, then the mrms between the obtained structure of Hb in the T-state and the reference structure in the R-state was calculated: mrms(I) = 3.15 Å and mrms(II) = 3.05 Å, (the mrms between the T and R crystal structures is 2.66 Å). The oxygen molecules ($O_2$) of the reference (R) were not taken into account.

Then followed 10 ps of productive dynamics simulations in which the PEDC constraints were applied to maintain the structure at approximately the same mrms distance from the reference (Fig. 1). However, because the protein was always inside the flat bottom of the potential well during these simulations and therefore did not "feel" the constraint at all, this phase of the calculations, which we will call displacement 0 ($J = 0$, where $d_0^0$ (I) = 3.15 Å and $d_0^0$ (II) = 3.05 Å), can be seen as an unconstrained productive MD and considered as a free dynamics phase. Throughout the procedure, the PEDC constraints ($V_{dist}$, $V_{trans}$, and $V_{rot}$) were applied only to protein atoms; the force constants to prevent overall translation and rotation were $k_{trans}$ = 500 kcal/mol/Å$^2$ and $k_{rot} = 10^{-10}$ kcal/mol/Å$^2$, respectively, and the width of the potential well 2δd = 0.8 Å.

For the first displacement ($J = 1$), the mrms was decreased by $\Delta d$ = 0.3 Å, such that $d_1^0$ (I) = 2.85 Å and $d_1^0$ (II) = 2.75 Å. The driving phase involved 1.2 ps of simulation during which $k_{dist}$ took the values of 200, 500, 1000, 5000, $10^4$, and $10^6$ kcal/mol/Å$^2$, changing every 200 fs, to bring the protein into the potential well centered on $d_1^0$. The confinement phase that followed consisted of 9 ps of productive MD under PEDC constraints with $k_{dist} = 10^6$ kcal/mol/Å$^2$ to maintain the protein within the flat-bottomed potential well reached during the driving phase. The same procedure was repeated through the fifth displacement ($J = 5$) (i.e., $d_5^0$ (I) = 1.65 Å and $d_5^0$ (II) = 1.55 Å). Beyond this point, it became more difficult to displace the system, i.e., the driving-phase constraint energy increased significantly compared to the previous steps, although it was still no larger than 0.14 kcal/mol per degree of freedom of the protein. Thus, we modified the value of $\Delta d$ from 0.3 to 0.15 Å for subsequent displacements, the rest of the procedure remaining the same. Throughout both trajectories, the PEDC constraint energy in the confinement phase (as opposed to the driving phase) was maximally $10^{-3}$ kcal/mol per degree of freedom of the protein, when the system reached one of the walls of the well. Thus, 16 displacement phases (or intervals) were used to bring the protein within δd of the R state ($d_{16}^0$ (I) = $d_{16}^0$ (II) = 0 Å). Each trajectory, including the 7 ps of the heating phase, totaled 200 ps and required 1100 hours cpu on a CRAY C98.

## RESULTS

In a MD simulation, the movements of the protein appear rather chaotic. Thus, we considered significant only the results relative to events taking place in both dimers (although not necessarily at the same time) and in both trajectories. The time indicated throughout the article refers to our simulation time, and not to the real time of the T–R transition, because the dynamics were carried out under constraints.

### Potential energy profile

It is difficult to straightforwardly calculate an energy profile of the transition pathway of a protein calculated by MD in explicit solvent. The strategy generally used is to apply an implicit solvent model to configurations of the protein taken from the trajectories (Duan et al., 1998). We present in this section the potential energy profile of Hb in which the solvent effects are taken into account by using a distance-dependent dielectric constant. Such an implicit solvent representation can overestimate electrostatic energies, but our purpose here is only to present a rough estimation of the potential energy along the transition trajectories to see whether the use of PEDC has introduced artefactual energy barriers.

In Fig. 2, we can observe that, for both trajectories, the potential energy of the protein is almost stable until ~57 ps (corresponding to the end of displacement $J = 3$), at which point it starts to increase, reaching a plateau at ~100 ps (end of $J = 7$). The large energy difference between these two points is mainly due to the overestimation of electrostatics as mentioned above. At the end of the trajectories ($t > 165$ ps, corresponding to the last 3 intervals of displacements), one can see that, in each driving phase leading to the next interval (see Methods), the potential energy of the protein increases and then decreases as it relaxes during the confinement phase. At this stage of the trajectories, it would appear that the confinement phase is not long enough to

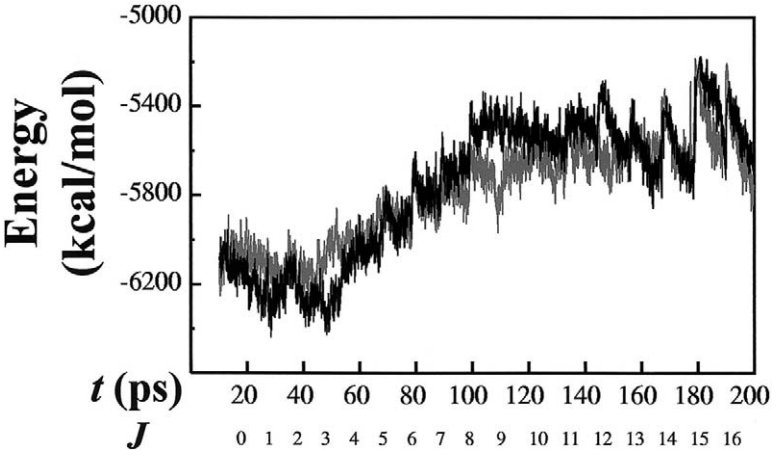


FIGURE 2 Potential energy of the protein alone calculated with a distance-dependent dielectric constant. The results are presented for all instantaneous structures along TrajI in black and TrajII in gray. For the abscissa, a double graduation is adopted: simulation time ($t$) in ps, and $J$, the number of intervals of displacement. In this and all following figures, the results are shown starting from the end of the 7-ps heating phase.

allow a complete relaxation of the protein. However, this is of no consequence for the structural analyses that follow, because, in the last three displacements ($J = 14–16$) the protein is already within fluctuation distance from the reference structure.

## Global analysis

Analysis of the structural modifications along the trajectories showed that the T–R transition could be divided into two major steps: the first step involving the quaternary transition (i.e., the rotation of one $\alpha\beta$ dimer with respect to the other), and the second step being the tertiary transition (i.e., the internal modifications of each $\alpha$ or $\beta$ chain to give the R-state). Indeed, as shown in Fig. 3, the rotation of the dimers was almost completed (i.e., dimer rotation angle $\theta$ relative to R reduced almost to 0°) when the rms deviation of the subunits from their tertiary R structures started to decrease—at 67 ps (beginning of interval $J = 5$) for the $\alpha$ chains and a bit later (77 ps, beginning of interval $J = 6$) for the $\beta$ chains. However, this does not mean that the chains behaved as rigid bodies in the first part of the transition. Indeed their rms with respect to the T structure increased from the beginning of the transition, but their internal modifications did not start to bring them close to the R structure until the quaternary transition was almost completed.

In TrajI, rotation of the dimers started spontaneously. The system did not feel the energy of constraint in the first displacement ($J = 1$, 27 ps $< t \leq$ 37 ps) because it had already reached the first intermediate mrms window in the unconstrained step ($J = 0$). In addition, for the next displacement ($J = 2$), the energy of constraint to bring the system into the window (see Fig. 1) did not exceed 7 kcal/mol. This constraint energy, which is global (i.e., not localized in any particular part of the protein) represented a negligible perturbation for the protein as it corresponded to less than one thousandth of its total energy ($4 \times 10^{-4}$ kcal/mol per degree of freedom), and it lasted less than half a picosecond. This shows that the quaternary transition may take place easily in the T state, confirming the results obtained previously by normal-mode (NM) calculations, which yielded a single low-energy mode corresponding mainly to the quaternary rotation (Mouawad and Perahia, 1996).

In contrast, in TrajII, in the free dynamics phase ($J = 0$, 17 ps $< t \leq$ 27 ps), dimer rotation began in the opposite direction from that required for the R structure. Thus, in the first displacement phase ($J = 1$), constraint was necessary to bring the structure closer to the reference. Indeed, in this trajectory, the energy of constraint was greater than zero during the whole driving phase (1.2 ps), although with a maximum of only about $10^{-3}$ kcal/mol per degree of freedom. However, as seen in Fig. 2, for both TrajI and TrajII, the overall energy profile, up to ~60 ps, is essentially flat.

## Movement of the helices

Visually, it is clear that the axis of rotation of one dimer is very close and parallel to the axis of its $\alpha$G helix (Fig. 4). This was confirmed by projection of the axis of the $\alpha$G helix onto the rotation axis of the corresponding dimer. This projection, after normalization of the two vectors, was close to unity along both trajectories.

To describe the movement of the helices of the protein over time, we calculated the angle between each helix axis at time $t$ relative to its corresponding axis in the T structure (here, the 7-ps structure at the beginning of free equilibration) after superimposition of the relevant chain (results not shown). In the $\alpha$ chains, the C helix underwent the largest movement, which started in the beginning of the transition. The F helix moved to a lesser extent, and the other helices did not move significantly. In the $\beta$ chains, the amplitude of the movement of the D and F helices was greater than that of the C helix, and the movement of the other helices was not significant. Interestingly, in the $\beta$ chains, the system behaved as if the amplitude of the C helix movement was

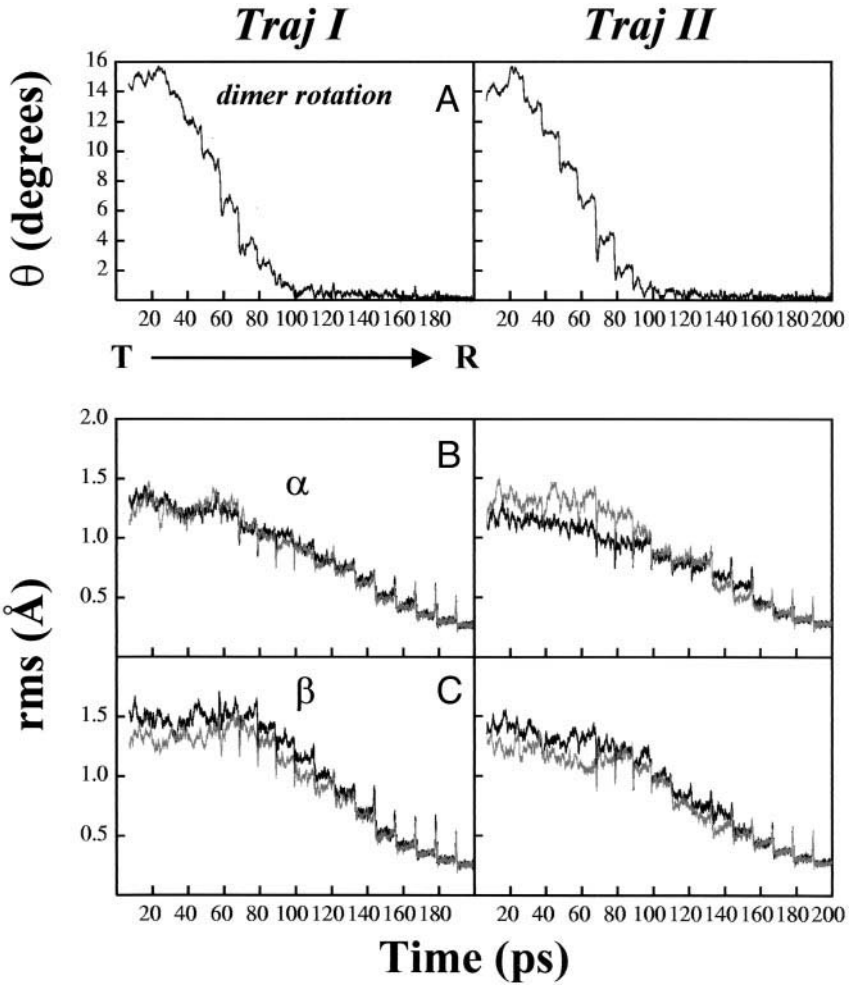


FIGURE 3 (*A*) The dimer rotation angle $\theta$, defined as the angle required to superimpose dimer $\alpha 2\beta 2$ of a given structure of human hemoglobin on that of the R state structure after initially superimposing their $\alpha 1\beta 1$ dimers. (*B*) $C_\alpha$ atom rms deviation for each $\alpha$ chain along the trajectory from the $\alpha$ chain in the R structure after their superimposition ($\alpha 1$, *black*; $\alpha 2$, *gray*). (*C*) Same as in (*B*) for the $\beta$ chains ($\beta 1$, *black*; $\beta 2$, *gray*).

diminished by the presence of the D helix, which has no equivalent in the $\alpha$ chains.

## Comparison with rigid-body rotation

We investigated possible factors impeding or favoring simple rigid-body rotation of the dimers. Independently of the calculated PEDC-MD trajectories, we carried out a rigid-body rotation (RBR) of one dimer with respect to the other and calculated, for each degree of rotation, the distances between the $C_\alpha$ atoms of the contact residues at the $\alpha 1\beta 2$ and $\alpha 2\beta 1$ interfaces. More precisely, the rigid-body movement consisted of rotation of one dimer with respect to the other, accompanied by a small translation of that dimer to bring the quaternary T structure close to the R form. For the sake of simplicity, however, this rigid-body movement will be referred to as rotation.

Various pairwise residue distances at the interdimer interface were calculated as a function of the RBR angle $\theta'$. To compare the RBR distances with those obtained along the calculated PEDC-MD trajectories, they are expressed as a function of time using the correspondence between angles $\theta'$ and $\theta$ to obtain the equivalent time from Fig. 3 *A*. Some typical curves are shown in Fig. 5.

As can be seen in Fig. 5 for the residue pair $\alpha 1(\alpha 2)$Pro-44(CE2) and $\beta 2(\beta 1)$His-97(FG4), several distance curves taken from the PEDC-MD trajectories corresponded well, or with a short time-lag, to RBR, suggesting that modification of the distance between these regions is similar to that of a simple dimer rotation. Interestingly, some of the other curves were very different, such as those referring to the "flexible joint" region consisting of the $\alpha$FG corner and the $\beta$C helix (Fig. 6). More precisely, the curves in Fig. 5, corresponding to the $C_\alpha$ distance between $\alpha 1(\alpha 2)$Asp-94(G1) and $\beta 2(\beta 1)$Trp-37(C3), showed that the RBR distance decreased to 3.5 Å, whereas the distance seen in PEDC dynamics decreased only to 6 Å. Similar behavior was observed to a lesser extent for other amino-acid pairs in the flexible joint region, such as those involving residues 92, 93, and 95 in the $\alpha$ chains, and residues 40 and 43 in the $\beta$ chains. This implies that the residues in this region, especially $\alpha$Asp-94 and $\beta$Trp-37, are likely to impede simple rotation of the dimers and that this could be overcome by tertiary modifications of the subunits.


FIGURE 4 Representation of the $\alpha 1\beta 1$ dimer in the T (*white*) and R (*gray*) structures after superimposition of their $\alpha 2\beta 2$ dimers. Near coincidence of the rotation axis of the dimer with that of the $\alpha$G helix is observed. The gray arrow indicates the direction of the movement from T to R.

Another interesting case in which RBR yielded a distance curve significantly different from the corresponding PEDC result concerned the residues $\alpha$1Val-96(G3) and $\alpha$2Val-96(G3). Indeed, whereas RBR would increase the distance between the $C_\alpha$ atoms of these residues, in the calculated trajectories, this distance decreased to a minimum (at ~57 ps, $J = 3$) during dimer rotation and then increased to the distance given by the RBR. At the minimum distance in the PEDC-MD results, contact between valine side chains occurred.

### Interfaces $\alpha 2\beta 1$ and $\alpha 1\beta 2$

The major structural modifications in the T-to-R transition described in the literature concern the C-termini of the $\alpha$ and $\beta$ chains and the switch region, which consists of the C-helix of $\alpha 2(\alpha 1)$ and the FG segment of $\beta 1(\beta 2)$ (Figs. 5 *D* and 6). In the switch region, during the T–R transition, the relative position of $\beta$1His-97 (FG4) changes from between $\alpha$2Pro-44(CE2) and $\alpha$2Thr-41(C6) to the adjacent placement between residues $\alpha$2Thr-41(C6) and $\alpha$2Thr-38(C3). This movement is referred to here as the "switch transition"; it is shown in Fig. 7, in which the $\alpha$-chain C helices of several structures (at the ends of intervals $J = 0$ to $J = 16$) are superimposed. However, this representation can give the misleading impression that the $\alpha$2C helix is static and that only the $\beta$1His-97 moves. This is not the case because, as was mentioned above, the $\alpha$C helices were shown to be very mobile during the transition. Thus, Fig. 8 shows another representation in which the $\alpha$2C helix and its facing $\beta$1His-97 in the first half of the transition (snapshots taken at the ends of intervals $J = 0$ through $J = 7$) are represented on a grid in the absolute frame (i.e., with no superimposition). This shows that, in the first part of the transition, the $\alpha$2C helix is mobile and deformable, possibly inducing the shift of $\beta$1His-97(FG4). Indeed, in this representation, it is only in interval $J = 6$ (between 78 and 88 ps) that $\beta$1His-97 started to change its absolute position.

The distance between the centers of mass (CM) of side chains $\beta 1(\beta 2)$His-97(FG4) and $\alpha 2(\alpha 1)$Pro-44(CE2) (Fig.

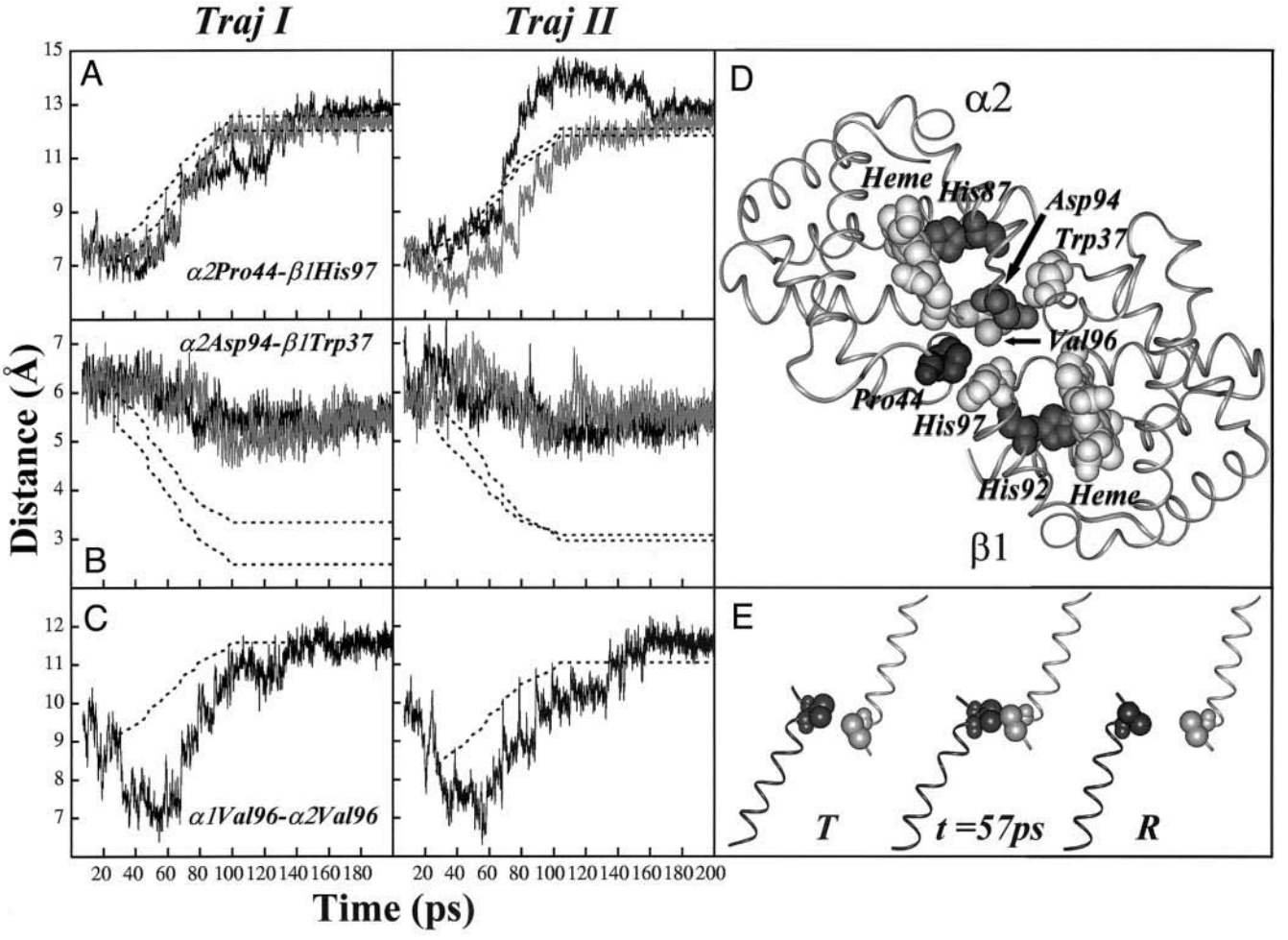


FIGURE 5 Distances across the dimer interface calculated along the PEDC-MD trajectories, between the $C_\alpha$ atoms of (*A*) $\alpha$1Pro-44(CE2) and $\beta$2His-97(FG4), (*B*) $\alpha$1Asp-94(G1) and $\beta$2Trp-37(C3), in which the black curve corresponds to interface $\alpha1\beta2$ and the gray curve to $\alpha2\beta1$, and (*C*) $\alpha$1Val-96(G3) and $\alpha$2Val-96(G3). In frames *A*, *B*, and *C*, the dashed curves correspond to the distances between these residues if the $\alpha2\beta2$ dimer is rotated as a rigid body with respect to $\alpha1\beta1$ (see the RBR procedure in text). For these curves, the angle of rotation was replaced by the corresponding time obtained *via* Fig. 3 *A*. (*D*) Representation of the $\alpha$2 and $\beta$1 subunits, with the residues listed above shown as hard spheres along with the proximal histidines (His-87 in $\alpha$ and His-92 in $\beta$) and the hemes. (*E*) The G helices (*ribbons*) and Val-96 (*hard spheres*) of $\alpha$1 (*gray*) and $\alpha$2 (*black*) are shown at three different points in the transition pathway, T ($t$ = 7 ps), R ($t$ = 200 ps), and $t$ = 57 ps (end of $J$ = 3). Note that, at $t$ = 57 ps, helix $\alpha$2G shows a slight deformation due to rotation of the first part of the helix as described in the Discussion.

9 *A*), started to increase at 67 ps (start of interval $J = 5$) due essentially to movement of the $\alpha$C helix itself. Note that, at this point, before the relative position of $\beta1(\beta2)$His-97(FG4) started to change, the dimer had rotated by $\sim11°$ ($\theta \approx 4°$, see Fig. 3 *A*). At the end of the switch transition ($J = 9$, 120 ps), when dimer rotation was essentially complete ($\theta < 2°$), the intrasubunit distance between the side chains CM of the $\beta$C-terminal residue His-146(HC3) and $\beta$Asp-94(FG1) began to increase significantly (Fig. 9 *B*). Finally, near the end of the trajectories (130 ps, end of $J$ = 10), the interdimer residues $\beta1(\beta2)$Trp-37(C3) and the $\alpha$C-termini $\alpha2(\alpha1)$Arg-141(HC3) started to separate (Fig. 9 *C*). This shows that there is a sequence of events that is well respected in both dimers and in both trajectories. We will see later that, in these trajectories, there appears to be a cause-and-effect relationship between these events.

### *Hydrogen bonds and salt bridges*

In the switch region, the energy of the hydrogen bond between $\alpha2(\alpha1)$Thr-41(C6) and $\beta1(\beta2)$His-97(FG4) was calculated along the trajectories (Fig. 10). We found that, in the $\alpha1\beta2$ interface, a strong hydrogen bond formed between these residues during the switch transition of $\beta$2His-97(FG4), whereas at the corresponding $\alpha2\beta1$ interface, this hydrogen bond formed only after the relative transition of $\beta$1His-97 was completed. More generally, during the transition of $\beta$His-97 (i.e., between 67 and 120 ps), the inter-

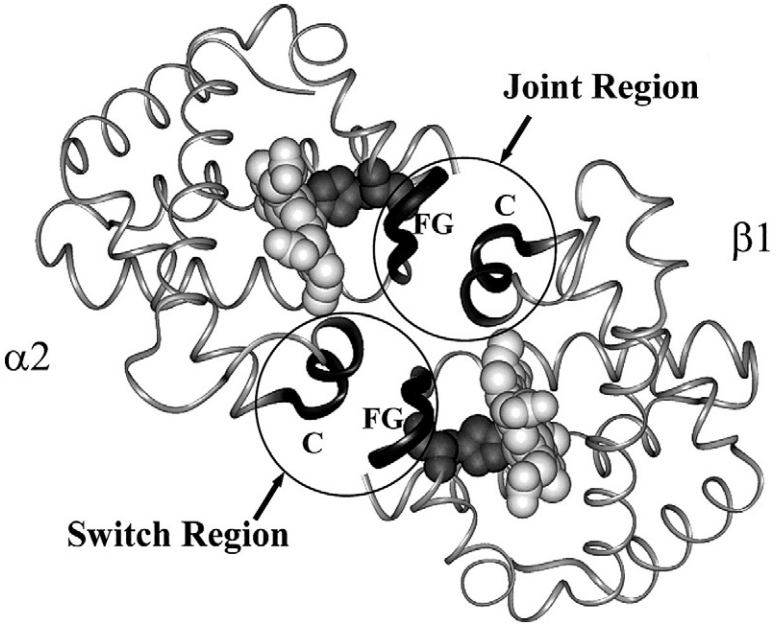


FIGURE 6 Representation of the $\alpha 2$ and $\beta 1$ subunits, with the proximal histidines and hemes shown as hard spheres. The joint region consists of the $\alpha 2$FG segment and the $\beta 1$C helix and the switch region consists of the $\alpha 2$C helix and the $\beta 1$FG segment.

action energy (and not only the hydrogen bond energy) between this residue and $\alpha$Thr-41(C6) was always attractive at the $\alpha 1\beta 2$ interface, whereas it was, at times, repulsive at the $\alpha 2\beta 1$ interface (results not shown), suggesting that there are different ways for the system to undergo this transition.

In contrast, the hydrogen bond between $\alpha 2(\alpha 1)$Tyr-42(C7) and $\beta 1(\beta 2)$Asp-99(G1), which is characteristic of the T-state, largely resisted dimer rotation, although it did display fluctuation. It broke definitively after the dimer rotation angle $\theta$ decreased to less than 4°. Another T-state

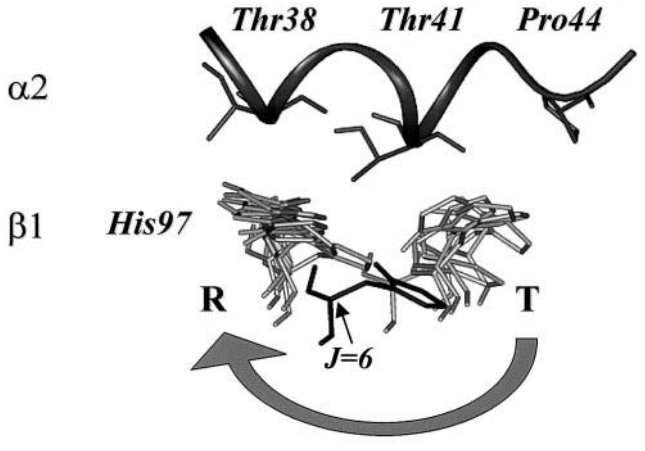


FIGURE 7 Snapshots of the switch region taken at the ends of the 16 intervals of displacement, in which each of the $\alpha 2$C helix (*dark gray*) was superimposed on that of the T state (only the T-state helix is shown). $\beta 1$His-97(FG4) from these timepoints and from T are drawn (*light gray*). The histidine resides most of the time either in the T conformation (i.e., between $\alpha$Thr-41 and $\alpha$Pro-44) or in the R conformation (between $\alpha$Thr-41 and $\alpha$Thr-38), with the transition taking place very rapidly, i.e., in only one interval ($J = 6$, between 78 and 88 ps, *black*).

hydrogen bond, between $\alpha 2(\alpha 1)$Asp-94(G1) and $\beta 1(\beta 2)$Trp-37(C3) (in the joint region), was much weaker but still resisted dimer rotation, at least at the $\alpha 2\beta 1$ interface. The hydrogen bond between $\alpha 2(\alpha 1)$Asp-94(G1) and $\beta 1(\beta 2)$Asn-102(G4) is usually described as characteristic of the R-state; Fig. 10 shows that it may exist at various stages of the allosteric transition, even in the T-state, though it is more frequent in the R-state. The strongest hydrogen bond (mean value −1.5kcal/mol) at this interface, which also resists dimer rotation, is between $\alpha 2(\alpha 1)$Arg-141(HC3) and the backbone of $\beta 1(\beta 2)$Val-34(B16).

Two salt bridges have also been described at this interface. In TrajI, both salt bridges $\alpha 2(\alpha 1)$Lys-90(FG2)–$\beta 1(\beta 2)$Glu-43(CD2) were disrupted more or less as a function of dimer rotation (Fig. 11 a, left). In TrajII, this salt bridge in the $\alpha 1\beta 2$ interface broke very quickly because, during the first half of this trajectory, $\beta$2Glu-43 interacted more strongly with the neighboring $\alpha$1Arg-92(FG4). In both trajectories and both dimers, when the system was close to the R state, $\alpha$Lys-90(FG2) rotated and established a hydrogen bond with one heme propionate of the same chain (not shown).

The second salt bridge is between $\alpha 2(\alpha 1)$Lys-40(C5), which is in the switch region, and the C-terminal carboxyl group of $\beta 1(\beta 2)$His-146 (Fig. 11 *A*, right). It broke entirely after ~120 ps ($J = 9$) because the $\beta$C-terminal histidine moved away from the $\alpha$-lysine (Fig. 11 b) as a result of the transition of $\beta 1(\beta 2)$His-97(FG4) from the $\alpha 2(\alpha 1)$Pro–Thr environment to the $\alpha 2(\alpha 1)$Thr–Thr environment (Fig. 7). This transition also induced the movement of $\beta 1(\beta 2)$Asp-94(FG1), releasing the terminal histidine (Fig. 9 *B*), which could then rotate easily to adopt its position in the R structure. This is why the C-terminal histidine (Fig. 9 *B*)

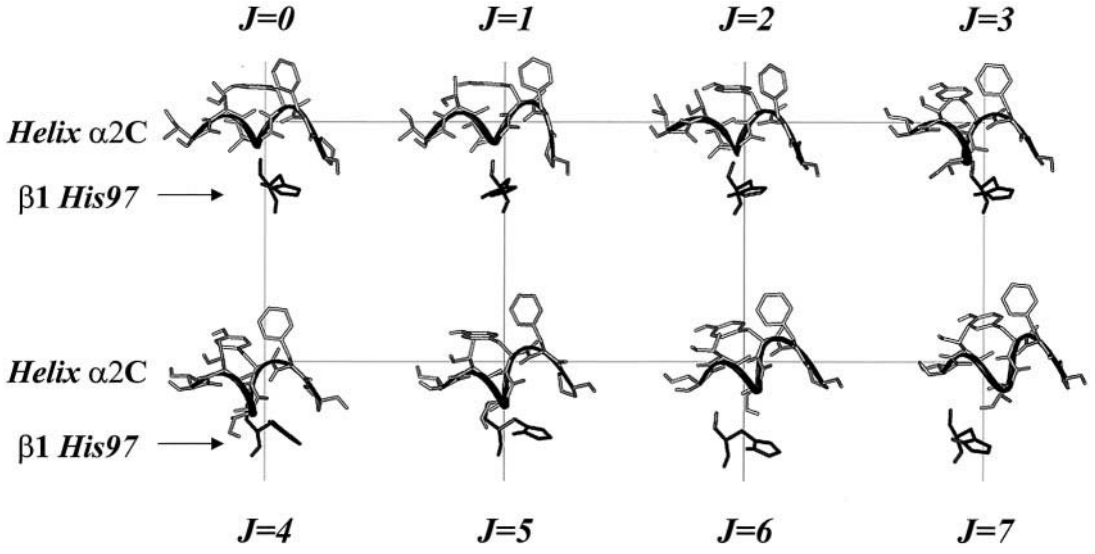


FIGURE 8 Snapshots of the switch region for the first half of the transition path, at the ends of displacement intervals $J = 0$ (T state) through $J = 7$ (98 ps), with **no** superimposition. The fixed grid is shown as a reference. In the first part of the transition path the $\alpha$C helix fluctuates, while the backbone of $\beta$His-97(FG4) maintains its absolute position until interval $J = 6$ (between 78 and 88 ps), where it starts its transition. Note that the residue's position is maintained throughout nearly the entire period in which dimer rotation occurs (see Fig. 3 *A*).

moved after the transition of $\beta$His-97(FG4) in the switch region (Fig. 9 *A*).

### Interfaces $\alpha1\alpha2$ and $\beta1\beta2$

The $\alpha1\alpha2$ interface was not significantly modified during the transition (Fig. 12), except that as the R structure was neared, the $\alpha$Arg-141 C-termini rotated and filled the space between the two chains. In contrast, the $\beta1\beta2$ interface showed extensive modification during the transition. Indeed, in the T structure, there is a wide cavity between the $\beta$ chains within which 2,3-diphosphoglycerate binds. This cavity closes upon dimer rotation, as shown in the structure at the end of $J = 6$ (88 ps) in which this rotation has already ended ($\theta < 2°$), but the $\beta$His-146 C-termini are still outside the cavity. Only after the hydrogen bonds between the $\beta$ chain C-termini and the $\alpha$Lys-40(C5) in the opposite dimer were broken at $J = 9$ (120 ps) did the histidine residues rotate to fill the remaining space in the cavity, as a consequence of the attraction by the N-terminal amino group of the facing $\beta$ chain.

### Interfaces $\alpha1\beta1$ and $\alpha2\beta2$

The $\alpha1\beta1(\alpha2\beta2)$ interface consists of helices B, G, and H in the $\alpha$ subunit facing helices H, G, and B in the $\beta$ subunit, respectively. The angles between the axes of the different helix pairs were calculated along the trajectories. Of these, the $\alpha$G–$\beta$G, $\alpha$G–$\beta$H, and $\alpha$H–$\beta$H helix angles showed significant transient deviations during the T–R transition. These movements are shown in Fig. 13. Although, in the other contacting helix pairs ($\alpha$B–$\beta$H and $\alpha$H–$\beta$B), such movements were less pronounced, they were still sufficiently large to induce transient contacts between certain residues at this interface, especially between $\alpha1(\alpha2)$Phe-36(C1) and $\beta1(\beta2)$Gln-131(H9).

### Environment of the hemes

#### *Distal environment of the hemes*

In the $\beta$ chains, the iron atom is hidden by the distal histidine (E7) and valine (E11) in the T state, which makes binding of the oxygen molecule more difficult than in the $\alpha$ chains (Fig. 14). In the R state (in which $O_2$ is bound but not shown in the Figure), these residues are pushed away. To characterize this movement, which is parallel to the heme plane, we calculated for both trajectories and for all chains the distances between the $C_\alpha$ atoms of the distal side residues and the normal to the best plane made by the four nitrogens of heme, this line passing through the Fe atom. In the $\alpha$ chains, these distances are approximately the same throughout the T-to-R transition (Fig. 15). In the $\beta$ chains, these distances are modified, reflecting the change in iron accessibility. For $\beta$His-E7 and $\beta$Val-E11, the distance to the heme normal is ~3.5 Å in the T state and increases during the transition to reach 5–5.5 Å in the R state. More precisely, this value is seen to increase at the end of dimer rotation (near 90–110 ps, or $J = 6–8$).

In the $\alpha$ subunits, there is apparently very little relative movement of the distal side residues with respect to the heme normal. In the $\beta$ subunits, the distances calculated for

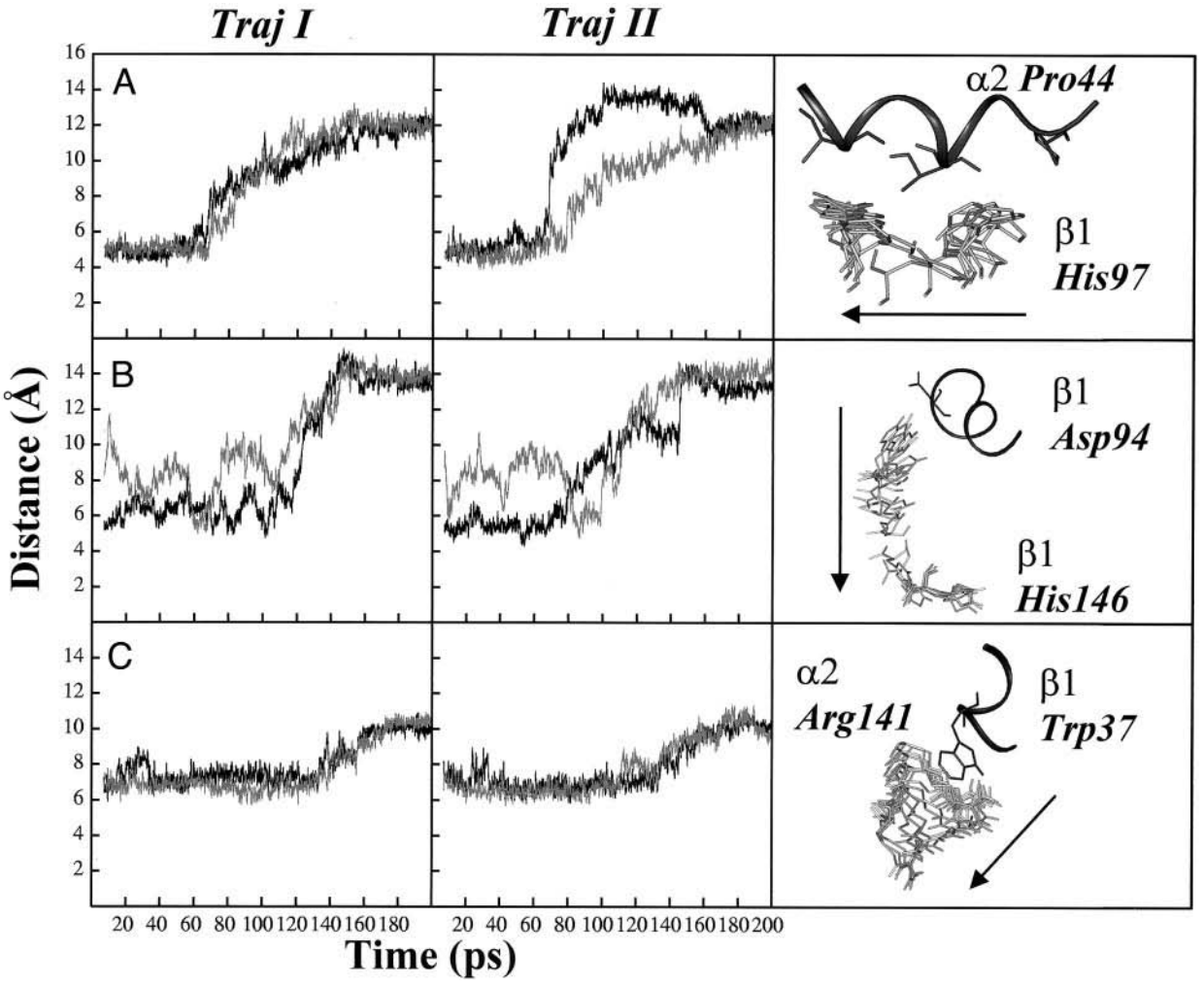


FIGURE 9 Distance between the side chain center of mass of the residues shown in the right-hand panels. (*A*) α2Pro-44(CE2)–β1His-97(FG4), (*B*) β1Asp-94(FG1)–β1His-146(HC3), and (*C*) α2Arg-141(HC3)–β1Trp-37(C3). The distances between α1 and β2 or between β1 and β1 are in black and the distances between α2 and β1 or between β2 and β2 are in gray. In the right-hand panels, the part of the subunit shown as a ribbon was superimposed on that of the T structure (only the latter is represented), and for the residue of interest, such as βHis-97, βHis-146, and αArg-141, the T structure and snapshots from the following 16 intervals of displacement are shown. The arrows indicate the direction of movement from T to R.

these residues showed an apparent correlation during the transition, although in some cases with opposite profiles. This indicates that either the distal side residues move together parallel to the heme plane in the subunit frame or the heme moves relative to them. In both cases, given the position of these residues encircling the normal to the heme plane (see Fig. 14, where this normal points from the Fe atom toward the reader), such a relative movement would bring the normal closer to some residues and away from the others. This explains why, in Fig. 15, the curve corresponding to Val-E11 (and to His-E7) in the β chains have a profile opposite from that of their neighboring residues.

In fact, these curves reflect movement of the heme within the β subunit, rather than movement of the whole set of distal side residues in concert. This is seen by examining the movement of the Fe atom itself relative to its position in the T state. In this analysis, for each α or β subunit, the structures along the trajectories were superimposed on the corresponding subunit of the T structure, and the distance between the Fe atom at each timepoint and its position in T calculated (curves in black in Fig. 15). The data show that, in the β subunits, the displacements of the Fe atom (black curves) are very well correlated with the distances of the distal residues from the normal of the heme plane (gray curves). This is not the case for the α subunits, where these distances are seen not to vary during the T–R transition. The same analysis but carried out for the $C_\alpha$ atoms of the different distal residues instead of the Fe atom showed no such correlation for either the α or β chains (data not shown).

Therefore, from the results presented in this section, we can conclude that, whereas in the α chain the Fe atom is

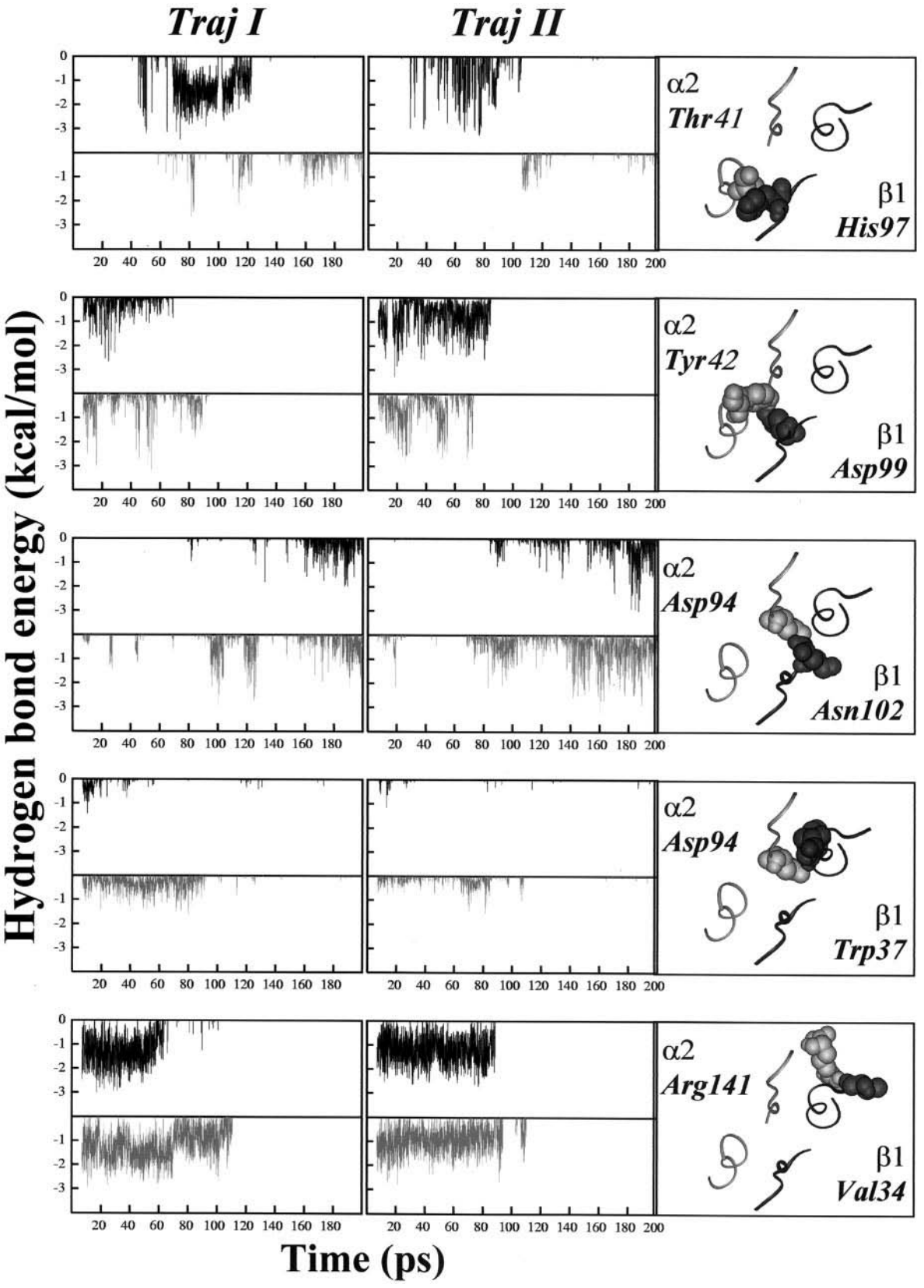


FIGURE 10 Hydrogen bond energy between residues at the $\alpha 1\beta 2$ (*black*) and $\alpha 2\beta 1$ (*gray*) interfaces. The $\alpha 2\beta 1$ interface in the T structure is represented in the right-hand panels, where the $\alpha$ and $\beta$ C helices and FG segments are shown as ribbons, and the two residues for which hydrogen bond energy is presented are shown as hard spheres.

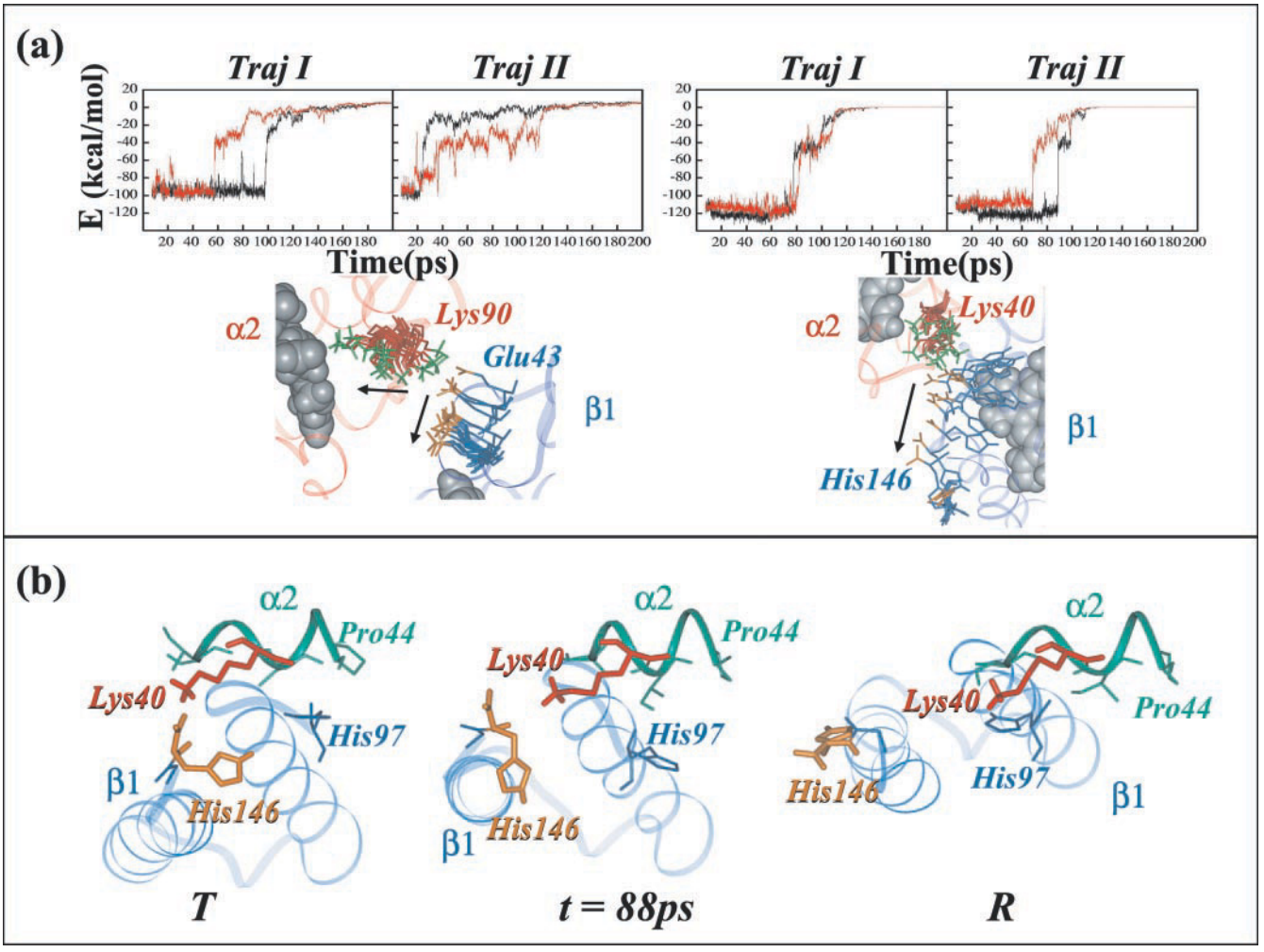


FIGURE 11 (*a*) Interaction energy between residues involved in salt bridges at the $\alpha 1\beta 2$ (*black*) and $\alpha 2\beta 1$ (*red*) interfaces. *Left*, $\alpha$2Lys-90(FG2) and $\beta$1Glu-43(CD2); *right*, $\alpha$2Lys-40(C5) and $\beta$1His-146(HC3). The T structure and snapshots from the following 16 intervals of displacement are shown. The residues are drawn in red with the amino group in green for $\alpha$, and in blue with the carboxyl group in orange for $\beta$. The arrows indicate the direction of movement from T to R. (*b*) Three snapshots corresponding to the T, the R, and the $t = 88$ ps (end of $J = 6$) instantaneous structures are shown. The $\alpha$2C helix is in green with its Lys-40(C5) in red, whereas the $\beta$1His-146(HC3) is in orange with $\beta$1His-97(FG4) and the segment connecting these two residues (i.e., helices G and H) in blue. This shows that, during the switch transition, $\beta$His-97 pushes away the $\beta$C-terminus, breaking the salt bridge between the terminal residue ($\beta$His-146) and $\alpha$Lys-40.

accessible to ligand even in the T state, in the $\beta$ chain the Fe atom becomes accessible during the transition not because of concerted movement of the distal side residues, but because of movement of the heme itself within the subunit.

### *Analysis in the frame of the heme*

To study in detail the motion of other residues around the heme in each subunit, each chain was considered independently, and the reference frame was modified to coincide with its heme. This treatment involved frame modification in the T structure, with each subunit rotated and translated to position the origin of the frame on the Fe atom (Fig. 16 a), the heme plane in the (X, Y) plane, the X axis approximately parallel to the F helix in the C- to N-terminal direction of the helix, and the Z axis pointing toward the distal side of the heme. In this representation, the Y axis points toward the interior of the subunit. As before, the instantaneous structures of each chain along a given trajectory were superimposed, using the $C_\alpha$ and Fe atoms, on the corresponding chain in the T structure in the new frame, and the coordinate differences calculated along the X, Y, and Z axes. The results are discussed below.

*Flexible joint region:* In the $\alpha 1\beta 2(\alpha 2\beta 1)$ flexible joint region, two residues of interest are $\alpha$1($\alpha$2)Asp-94(G1) and $\beta$2($\beta$1)Trp-37(C3). As shown above, a tertiary movement is important to prevent these two residues from colliding, as would occur with simple rigid-body dimer rotation. Analysis of these residues' movements along the X, Y, and Z axes (data not shown) demonstrated that $\alpha$Asp-94 moved in

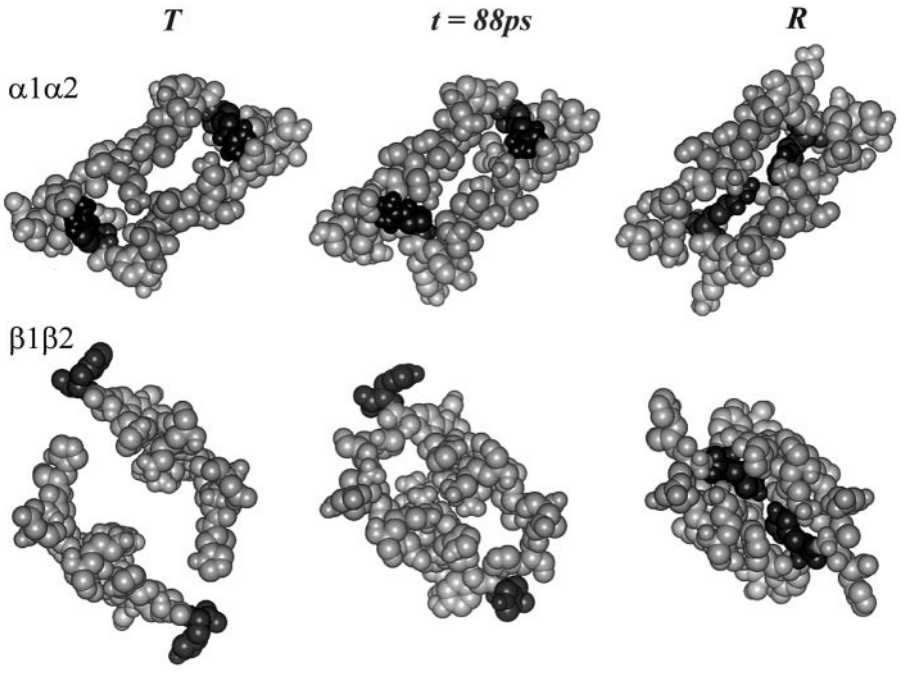


FIGURE 12 Three snapshots corresponding to those represented in Fig. 11 b (i.e., T, R, and $t = 88$ ps) but here with the $\alpha1\alpha2$ and $\beta1\beta2$ interfaces shown as hard spheres. The $\alpha$Arg-141 and the $\beta$His-146 C-termini are in black. The $\alpha1\alpha2$ interface can be seen to be relatively unmodified during the T–R transition, except for the $\alpha$C-termini that fit into this interface at the end of the transition. In the $\beta1\beta2$ interface, the closing of the cavity was seen to occur by 88 ps (i.e., during dimer rotation) with the C-termini still outside the cavity, after which the C-termini rotated and fit into the interface.

concert with the proximal histidine $\alpha$His-87(F8) of the same $\alpha$ chain, along either the X axis or the Z axis, depending on the subunit, but, in both cases, in such a way that collision with the $\beta$Trp-37 was prevented (Fig. 16 a). Movement of $\beta$Trp-37 is less significant, and is correlated with that of the proximal histidine $\beta$His-92(F8) of the same $\beta$ chain through the movement of the switch region and the neighboring $\beta$Asn-102(G4).

*Proximal side:* Figure 16 b shows movements along the X axis of the Fe atom and $C_\alpha$ atoms of the proximal histidine F8 and residue FG4. In the $\alpha$ chains, little or no movement was seen in this direction. In contrast, in the $\beta$ chains, after most of the rotation was accomplished ($\theta < 2°$, $J = 6$, $t = 88$ ps), the $\beta$His-FG4 of the switch region started to move along the X axis in the negative direction due to its displacement from the $\alpha$Pro–Thr environment to the $\alpha$Thr–Thr environment described earlier. As shown in Fig. 16 b, this movement along the X axis occurred in concert with that of the proximal $\beta$His-F8 and the $\beta$-heme, making the Fe atom accessible to the ligand. Indeed, as can be seen in Figs. 14 and 16 a (in which the hemes are shown in the same orientation), to release the Fe on its distal side, the heme must move in this frame along the X axis, parallel to the F helix, in the negative direction.

## DISCUSSION

This study of the T-to-R transition pathway of hemoglobin in water is composed of two PEDC-MD trajectories. The advantages of the present simulations are that the influence of water at ambient temperature was taken into account, and we have access to many transient and intermediate states allowing a detailed structural description of the transition. Because of the substantial computational expense involved due to the presence of explicit water molecules in the model, we chose as a target structure only the R state of Hb A, despite the fact that this is not necessarily the only ligated species that exists in solution (Mueser et al., 2000). We made this choice to be able to compare our results with the mechanism proposed by Perutz (1970) and Perutz et al. (1998) and with the large ensemble of experimental results based on the R structure. However, one should keep in mind that, if the reference were the R2 structure (Silva et al., 1992), or any of the other structures of fully liganded Hb A, the results could be noticeably modified.

The goal of this study is to describe in detail the structural modifications of Hb during the transition between the T and R structures. It does not pretend to give a minimum energy profile of the T-R pathway; for this we would have used PEDC in combination with EM instead of MD, as previously published by Guilbert et al. (1995). In fact, with this in mind, we minimized without constraints the energy of several structures taken from the calculated PEDC-MD trajectories (data not shown) and observed a reaction path similar to the one obtained previously by the PEDC-EM method (Guilbert et al., 1995). These results are also similar to those obtained by NM analysis (Mouawad and Perahia, 1996), demonstrating that the trajectories calculated here do not stray from the low-energy valley found by other methods.

The energy profile presented in the results (Fig. 2) provides a good means to monitor the relevance of our calculations because the trajectories are short (due to the large number of atoms), and thus the stresses involved in displac-

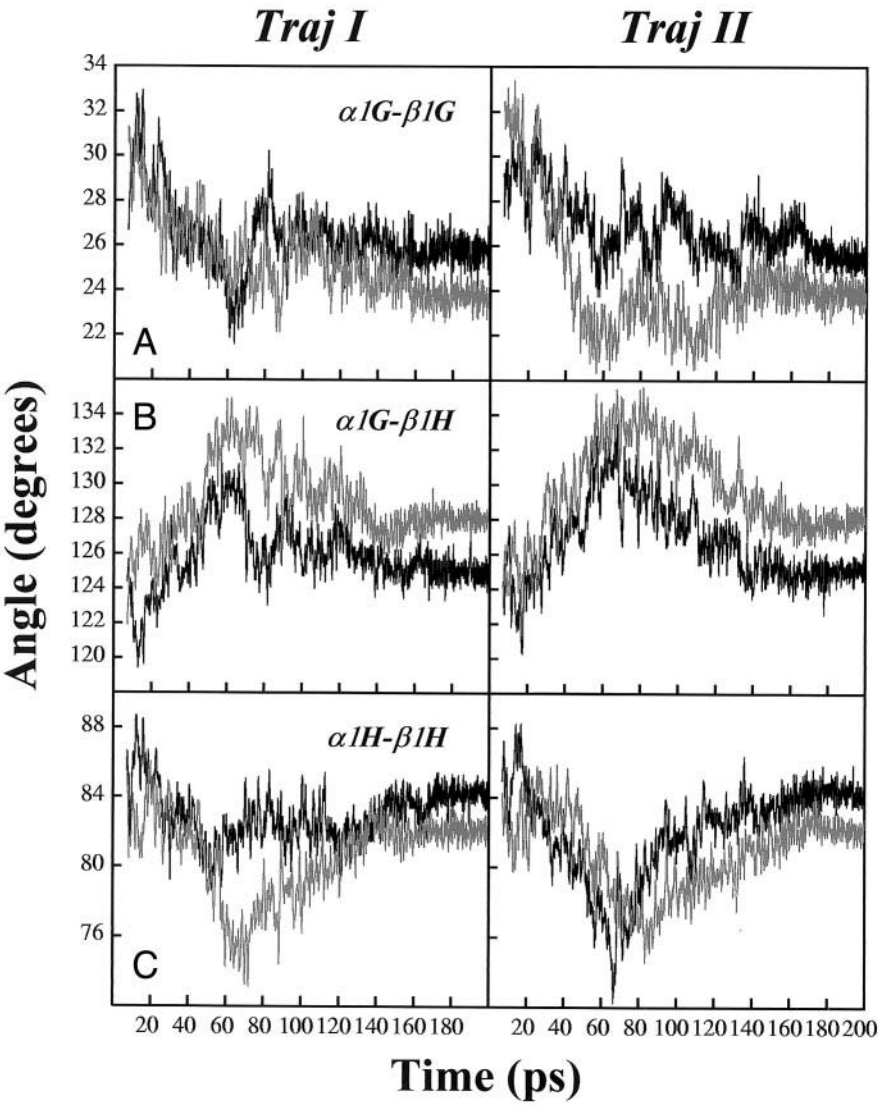


FIGURE 13 The angle between helix axes at the $\alpha 1\beta 1$ (*black*) and $\alpha 2\beta 2$ (*gray*) interfaces. (*A*) Angle between helices $\alpha$1G and $\beta$1G; (*B*) $\alpha$1G and $\beta$1H; and (*C*) $\alpha$1H and $\beta$1H. The other pairwise combinations involving contact helices B, G, and H showed no significant transient movement.

ing the structure toward the target could be rather severe. However, as one can see in Fig. 2, despite the large energy difference between the starting and ending points of the trajectories, the system is well behaved until the last three displacements ($J = 14–16$), where, as we mentioned before, the structure is already essentially in the R conformation. A detailed analysis of the energy difference between the start and the end of the trajectories shows it to be mainly due to the interdimer interactions, which are less numerous in the R structure than in T. It should, however, be noted that this energy is overestimated because of the approximate solvent model used in its calculation (see the Results).

The structural analysis of the calculated trajectories suggests that the allosteric transition may be divided into two major steps: the quaternary transition that begins easily (the energy profile in Fig. 2 is flat up to 60 ps) and even spontaneously (as in TrajI), followed by a tertiary transition to the R form (Fig. 3). However, the quaternary transition itself is accompanied by tertiary modifications that move each individual chain far from its T structure, although the rms deviation from R is not significantly affected. It is only after the dimer rotation is almost completed, $\theta \approx 4°$, that the rms of each chain with respect to the R structure starts to decrease. This could be due to the PEDC constraint, which may favor collective movements over local ones, allowing the system to reduce the rms difference with the least energy cost. However, as shown in the results, dimer rotation began in one trajectory before the system felt any PEDC constraints at all, showing that this movement may occur spontaneously at the start of the transition. Moreover, the division of the transition into two major steps was also observed in our previous results obtained by a completely different method: the NM analysis applied to hemoglobin in vacuum (Mouawad and Perahia, 1996). It is also consistent with experimental results showing the existence of an

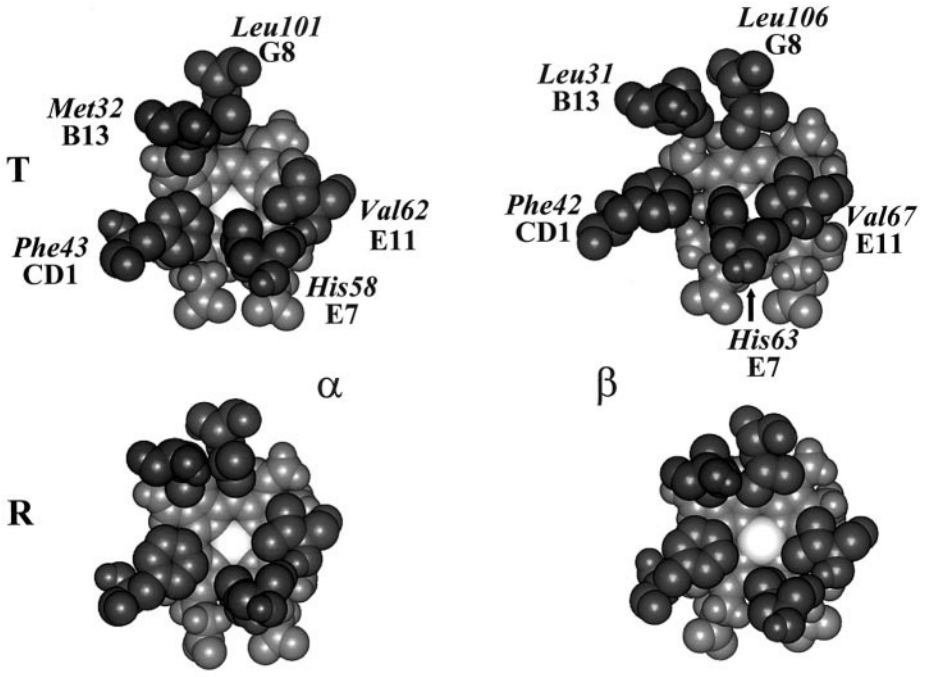


FIGURE 14 The distal side (*black*) of the $\alpha$ and $\beta$ subunits in the T and R conformations. The heme is in gray and the iron atom in white. The five residues (B13, CD1, E7, E11, and G8) that are in close contact with the heme on the distal side are shown as hard spheres. It can be seen that, in the T state, the Fe atom is more accessible to ligand in the $\alpha$ chains than in the $\beta$ chains.

intermediate state that is quaternary R-like (Eaton et al., 1991; Hofrichter et al., 1991; Henry et al., 1997).

### The interface between the dimers

Both this study and the NM analysis show that, in the absence of ligand, up to $\theta \approx 4°$ of relative dimer rotation (which corresponds here to displacements up to $J = 5$) can occur with a configuration of the $\alpha1\beta2(\alpha2\beta1)$ interface corresponding to the T state, and that it is only after the rotation is almost completed that tension in the switch region makes the switch transition possible. The structure and its modifications in the switch region are qualitatively symmetric in both dimers, which is to be expected because the transition in this region depends on rotation of the dimers with respect to each other.

In both PEDC-MD trajectories, the $\alpha$C-helix in the switch region moves and deforms slightly during the T–R transition, resulting in movement of the facing $\beta$His-97(FG4) and the $\beta$C-terminal histidine. The movement of the $\alpha$C-helix is itself correlated to dimer rotation. In NM analysis, this correlation can be seen clearly, because the tertiary movements associated with the mode corresponding to dimer rotation occur principally in the $\alpha$C-helix (unpublished results). In PEDC-MD trajectories, this correlation can be shown indirectly by calculating equal time correlation functions, $c$, between the $C_\alpha$ atoms of the $\alpha$C-helix and those at the start of the $\alpha$G-helix. As mentioned in the Results, dimer rotation occurs about an axis close to the $\alpha$G-helix axis, and because the dimer rotation is accompanied by rotation of the start of the G-helix about its own axis (Fig. 5 *E*), the internal movements of the $\alpha$ chain that are correlated to those of the start of the $\alpha$G-helix are considered to be correlated to dimer rotation. This analysis shows that movement of $\alpha$Asn-97(G4) was strongly correlated to that of residues near the end of the C helix of the same $\alpha$ chain, namely Tyr-42(C7) with $c = 0.94$ and Phe-43(CE1) with $c = 0.96$.

At the $\alpha1\beta2(\alpha2\beta1)$ interface, the hydrogen bonds and salt bridges that characterize the T state resist much of the dimer rotation until $\theta$ reaches 4°. The subunits thus demonstrate considerable elasticity, making it possible to maintain the conformation of the interface (in this case the T conformation) to a certain extent independently of dimer rotation. This has been observed experimentally by nuclear magnetic resonance (Fujii et al., 1993), with the porphyrin(PP)-iron hybrid hemoglobin $\alpha(Fe)_2\beta(PP)_2$ shifting to the R quaternary state upon CO binding, whereas the T-state marker consisting of the hydrogen bond between $\alpha$1Tyr-42(C7) and $\beta$2Asp-99(G1) did not completely disappear (although it was significantly reduced). The crystal structures of carbonmonoxide ligated crosslinked Hb show a quaternary R state but with the switch region shifted toward the T state (Schumacher et al., 1995).

As a corollary, it follows that experimental observation of the $\alpha1\beta2$ and $\alpha2\beta1$ interfaces alone does not necessarily

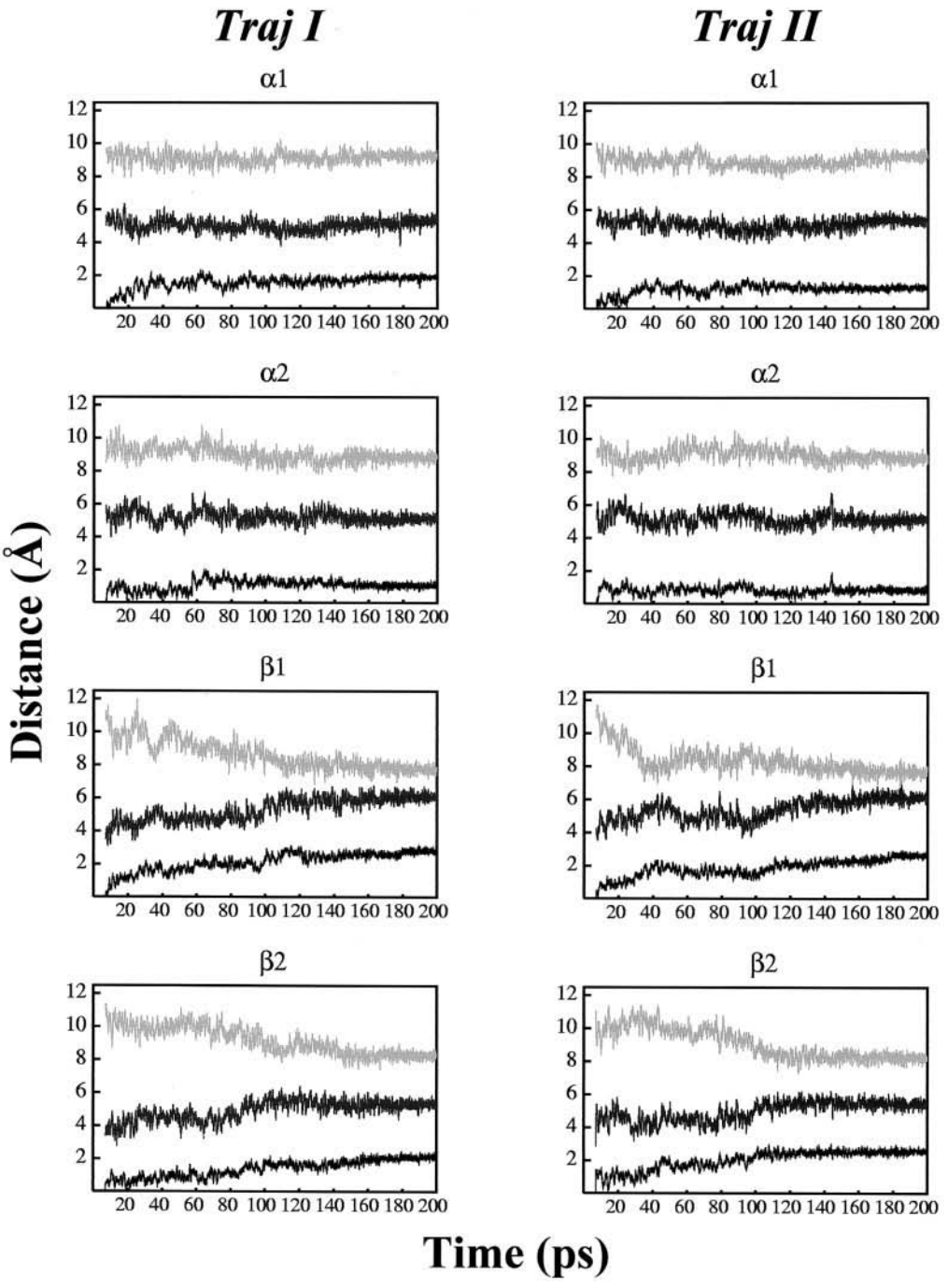


FIGURE 15 Distances from the normal of the heme plane (passing through the Fe atom) to the $C_\alpha$ atom for the five residues of the distal side shown in Fig. 14. For each chain, only the curves corresponding to residues CD1 (*light gray, top curve*) and E11 (*dark gray, middle curve*) are represented for clarity. The curves for residues B13 and G8 were almost coincident with that for CD1, and the curve for E7 was almost coincident with that for E11. The bottom curve (*black*) for each chain corresponds to the distance between the Fe atom in each instantaneous structure along the trajectory and the Fe atom of the same chain of the T structure, after superimposition of the $C_\alpha$ and Fe atoms of the corresponding chain.

reveal the relative positions of the dimers. Indeed, for the same conformation of this interface, a certain range of dimer rotation should be possible; this is reflected in the spontaneous dimer rotation seen at the beginning of TrajI, and in the natural propensity for the quaternary movement in the deoxy molecule that was demonstrated previously by NM analysis (Mouawad and Perahia, 1996).

In both trajectories, a chronology of events at this interface was well respected and can be described as follows. In the first part of the dimer rotation, the $\alpha$C-helix fluctuates

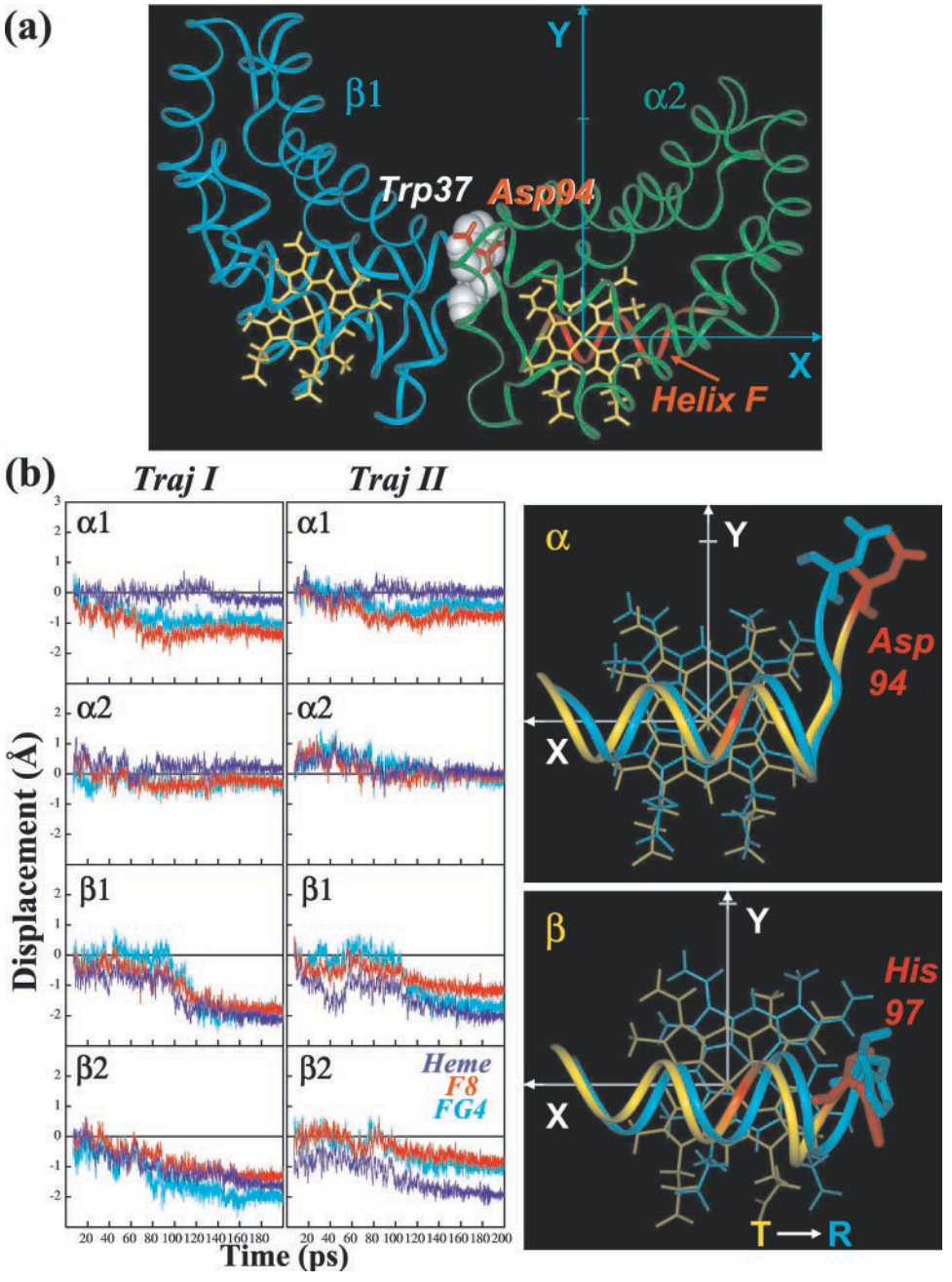


FIGURE 16 (*a*) Representation of the T-state α2 (*green*) and β1 (*blue*) subunits, in the reference frame used to interpret movements in the heme region. As shown here for α2, each subunit of the T-state protein is reoriented independently such that the origin is at the Fe atom (the heme is *yellow*), the X-axis is approximately parallel to the axis of the F helix (*red*), running from the C- to the N-termini of the helix, the Y axis points toward the interior of the subunit, and the Z axis points toward the distal side of the heme (i.e., toward the reader). In the flexible joint region, α2Asp-94 is shown as red wireframe and β1Trp-37 as hard white spheres. (*b*) Atom displacements relative to T in the instantaneous structures, obtained by superimposition of each subunit on the corresponding one in the T structure in the frame described above. The displacement along the X axis of the atom of interest at each timepoint from its position in the T structure was calculated. These displacements were calculated for the Fe atom (*dark blue*) and for the $C_\alpha$ atoms of the proximal histidine, F8 (*red*), and for residue FG4 (*cyan*, Arg-92 in α and His-97 in β). The right-hand panels, showing each subunit in the reference frame described in (*a*) but viewed from the proximal side, represent the F helix and the heme for the T (*yellow*) and R (*blue*) structures. It can be seen that, in β, the F helix and the heme move in the negative direction along the X axis, whereas in α no significant movement is observed along this axis. In the T structure of both α and β, the portion of the helix corresponding to the proximal histidine (F8) is shown in red. The FG4 residue is only represented in the β subunit (His-97, *red* in T, *blue* in R), as in α it undergoes no significant movement. In the α subunit, we also show Asp-94(G1) (*red* in T, *blue* in R), the movement of which is described in the text.

and induces βHis-97(FG4) in the switch region to pass from its position between αThr-41 and αPro-44 to that between αThr-41 and αThr-38. This has two complementary effects leading to the release of the βC-terminal histidine. First, the movement of the backbone around βHis-97(FG4) removes βAsp-94(FG1) from the vicinity of βHis-146(HC3) (Fig. 9*B*), breaking the hydrogen bond between these residues that had stabilized the T structure. Second, the new position of βHis-97(FG4) displaces on the βC-terminal histidine, breaking its carboxy terminal salt bridge with αLys-40(C5) as shown in Fig. 11. When βHis-146(HC3) is released, it moves toward the amino group of the now nearby N-terminal valine of the other β chain, which has moved closer with the dimer rotation, then rotates and fills the space between the two β chains.

On the opposite side of the protein (i.e., at the αC-terminus), because of dimer rotation and tertiary readjustment in the chains, the environment of αArg-141(HC3) becomes more positive, resulting in repulsive interactions with the arginine, inducing its rotation to fill the space between the α1 and α2 chains. In the absence of chloride ions in the simulations, the salt bridge between the α1N-terminus and α2C-terminus was maintained throughout the T-to-R transition.

Despite fluctuations in the αC-helix and tertiary readjustment in the subunits, we saw that the transition of the switch region could be accounted for essentially by rigid-body rotation of the dimers. In contrast, in the flexible joint region, rigid-body dimer rotation would fail because of the absence of internal movement of the subunits. The movements necessary to prevent this blockage are those of αAsp-94(G1) and βTrp-37(C3). Each of these residues was shown to move in concert with the proximal histidine (F8) of its own chain, suggesting that ligand binding can affect this interface.

We also asked whether the influence of the F8 histidines extended across the flexible joint interface, i.e., whether, α1Asp-94 was correlated with β2F8, and whether, correspondingly, β2Trp-37 was correlated with α1F8. Interestingly, this correlation is much higher in the latter case, with $c = 0.86$, than in the former, with $c = 0.54$. This may explain why replacement of the β-chain Trp-37 in the interface by different residues (Tyr, Ala, Gly, or Glu) results in structural modifications in the α chain F-helix and, for the βW37G and βW37E mutants, shortening of the Fe-$N_{\varepsilon 2}$His(F8) bond in the α subunit as well as in the β subunit (Peterson and Friedman, 1997; Kavanaugh et al., 1997).

The slight rotation of the start of the αG-helix mentioned above helps to prevent collision between αAsp-94(G1) and its facing βTrp-37(C3) during dimer rotation. This movement of the αG-helix is also responsible for decreasing the distance between the Val-96(G3) residues of the two α chains, which does not occur with rigid-body rotation. Contact between these two residues, together with their proximity to the heme, may be part of an explanation for the observed cooperativity of hybrid molecules, in which the Fe atom is replaced in the β subunits by another metal atom so that ligand can bind only to the α subunits (Fujii et al., 1993; Shibayama et al., 1995a,b).

## Interfaces α1β1 and α2β2

The PEDC-MD analysis revealed transient effects that would be very difficult to observe experimentally, especially at the α1β1(α2β2) interface (Fig. 13). Indeed, the α1β1 and α2β2 interfaces were found here to be less rigid than previously estimated (Baldwin and Chothia, 1979). Transient readjustment of the helices in these interfaces was observed during dimer rotation. When the rotation is almost finished ($\theta$ between 4° and 6°, in intervals $J = 4, 5$) and when the interdimer α1β2 and α2β1 interfaces start to be modified (in intervals $J = 5, 6$), the helices in the intradimer α1β1 and α2β2 interfaces begin to return to their initial relative position. Thus, it is as if during dimer rotation, preservation of the structure of the interdimer (α1β2 and α2β1) interfaces is made possible by transient modification of the intradimer interfaces.

## The heme environment

Analysis of the environment of the hemes showed that, in the α subunits, the heme does not undergo an important overall movement with respect to the polypeptide chain during the T-to-R transition. This is to be expected because its position in the T structure already allows ligand binding. Its open conformation in the T structure may appear to be due to the presence of a water molecule on the distal side of both α-hemes in the crystal structure of deoxyHb that we used (PDB dataset 2HHB (Fermi et al., 1984)). However, in all the crystal structures of deoxyHb in the protein database, there is a water molecule on the distal side of the heme of at least one α subunit but not of any β subunits. Thus the argument may be turned around such that water molecules are present in these positions because there is already enough space. This is supported by the observation in the PEDC-MD trajectories of a large cavity on the distal side of the α-heme that forms spontaneously in the T state, in interval $J = 0$ (manuscript in preparation). Conversely, the distal side of β-hemes is more closed in the T state, providing a rationale for the observation that the affinity of these chains in the T-state is three times lower than that of the α-chains (Zhou et al., 1991; Shibayama et al., 1995a). During the T-to-R transition, the distal side of the β-hemes opens with the switch transition. Indeed, we found that, toward the end of the dimer rotation, the βHis-97(FG4) of the switch shifts from the αThr–Pro to the αThr–Thr environment, and the β-proximal histidine βHis-92(F8) and β-heme follow this movement. Translation of the β-heme toward the βFG corner opens the distal side, making the

iron atom accessible to the ligand. This movement also straightens the β-proximal histidine and pushes the iron toward the plane of the porphyrin.

### Mechanistic aspects of the allosteric transition

Our observations of the detailed atomic-level movements revealed by the PEDC-MD trajectories lead us to propose a new chronology of events for the mechanism of T-to-R transition that is consistent with the Perutz mechanism, but in which the roles played by the various regions of the protein are different. In the absence of ligands, T-state Hb would appear to have a natural propensity for dimer rotation (Mouawad and Perahia, 1996; this work), which would be hampered by αAsp-94(G1) and βTrp-37(C3) in the joint region of the $\alpha1\beta2$ interface. The correlation between the movements of αAsp-94(G1) and proximal histidine αHis-87(F8) suggests that the presence of bound ligand at the α-hemes may release the joint region, allowing the rotation to continue. This is consistent with the modifications described at this interface in the crystal structure of the fully liganded T state Hb (Paoli et al., 1996). The release must happen on both sides ($\alpha1\beta2$ and $\alpha2\beta1$) or else the rotation would not be able to proceed.

This chain of events in the joint region is consistent with several experimental findings. First, the binding of two ligands to the α subunits appears to induce the quaternary transition (Ogawa and Shulman, 1972; Di Cera et al., 1987; Fujii et al., 1993; Kiger et al., 1993; Shibayama et al., 1995a, b; Unzai et al., 1998). Second, based on NMR studies of βTrp-37, Mihailescu et al. (2001) proposed that the joint region is important in the transduction of binding free energy into the structural modifications essential for cooperativity. Third, decoupling of the proximal histidine connection to the Fe atom in the α subunits leads to retention of the T-quaternary structure in the fully liganded Hb (Barrick et al., 2001), presumably reflecting a flawed linkage between ligand binding and the release of the joint region. In the β subunits, proximal histidine decoupling did not lead to a similar effect.

After release of the joint region, and as the dimer rotation continues, the αC-helix (the movement of which is correlated to the quaternary transition) generates strain on the β side of the switch region, leading the βHis-97(FG4) to advance one turn in front of the αC-helix. This movement has two effects: (1) it removes the βC-terminus from the vicinity of αLys 40(C5) and shifts the backbone between residues βHis-92(F8) and βHis-97(FG4) such that the hydrogen bond that links βAsp-94(FG1) to the βC-terminal histidine is broken, releasing the latter; and (2) it helps to translate the heme toward the βFG corner, making the iron atom accessible to ligand, thereby probably increasing the affinity of the protein. This last assumption is consistent with the observation that the R-like deoxy $\beta_4$-homotetramer, which has an affinity as high as that of the R state of hemoglobin, shows the distal side of all four β-chain hemes to be in an open conformation (Borgstahl et al., 1994).

## CONCLUSION

We used MD and the PEDC method to investigate the transition pathway from the T to the R state of hemoglobin. Our results led us to propose a mechanism for the allosteric transition consistent with the mechanism put forward by Perutz (1970) and Perutz et al. (1998) in the sense that the same regions of the protein are considered to play an important role in the T–R transition. However, the function of residues in these regions is different from that proposed by Perutz. Indeed, in our description, the dimer rotation is not induced directly by ligand binding, but the protein has a natural propensity for this movement, which is simply limited in scope by the aminoacid backbone in the joint region. The role of the ligand binding is thus to release this region and allow completion of the dimer rotation. In contrast, as with the Perutz mechanism, we consider that the opening of the β distal side may be crucial for increasing oxygen affinity. However, this opening is shown here not to be due to movement of the distal side of the heme as was initially proposed, but rather to movement of the heme itself, which is correlated to movement of the switch region in the $\alpha1\beta2(\alpha2\beta1)$ interface.

Moreover, this analysis demonstrates the presence of elasticity through which the T conformation of the interdimer interface ($\alpha1\beta2$ or $\alpha2\beta1$), with its network of hydrogen bonds and salt bridges, can be maintained, to a certain extent, during dimer rotation. A similar property was also observed recently in the R structure by (Mueser et al., 2000). This elasticity is probably linked to the transient modifications observed in the intradimer interfaces ($\alpha1\beta1$ and $\alpha2\beta2$), giving a possible explanation to the role of mutations at this interface.

This work was supported by the Centre National de la Recherche Scientifique (CNRS) and the Institut National de la Santé et de la Recherche Médicale. The simulations were performed on the CRAY C98 of the IDRIS supercomputer center of the CNRS.

## REFERENCES

Baldwin, J. and C. Chothia. 1979. Haemoglobin: the structural changes related to ligand binding and its allosteric mechanism. *J. Mol. Biol.* 129:175–220.

Barrick, D., N. T. Ho, V. Simplaceanu, and C. Ho. 2001. Distal ligand reactivity and quaternary structure studies of proximally detached hemoglobins. *Biochemistry.* 40:3780–3795.

Bernstein, F. C., T. F. Koetzle, G. J. B. Williams, E. F. Meyer, M. D. Brice, J. R. Rodgers, O. Kennard, T. Shimanouchi, and M. Tasumi. 1977. The protein data bank: a computer-based archival file for macromolecular structures. *J. Mol. Biol.* 112:535–542.

Borgstahl, G. E. O., P. H. Rogers, and A. Arnone. 1994. The 1.9Å structure of deoxy $\beta_4$ hemoglobin. Analysis of the partitioning of quaternary-

associated and ligand-induced changes in tertiary structure. *J. Mol. Biol.* 236:831–843.

Brooks, B., R. Bruccoleri, B. Olafson, D. States, S. Swaminathan, and M. Karplus. 1983. CHARMM: a program for macromolecular energy, minimization, and molecular dynamics calculations. *J. Comp. Chem.* 4:187–217.

Bruno, S., S. Bettati, M. Manfredini, A. Mozzarelli, M. Bolognesi, D. Deriu, C. Rosano, A. Tsuneshige, T. Yonetani, and E. R. Henry. 2000. Oxygen binding by $\alpha(Fe^{2+})_2\beta(Ni^{2+})_2$ hemoglobin crystals. *Prot. Sci.* 9:683–692.

Csajka, F. S., and D. Chandler. 1998. Transition pathways in a many-body system: application to hydrogen-bond breaking in water. *J. Chem. Phys.* 109:1125–1133.

Di Cera, E., C. H. Robert, and S. J. Gill. 1987. Allosteric interpretation of the oxygen-binding reaction of human hemoglobin tetramers. *Biochemistry.* 26:4003–4008.

Duan, Y., L. Wang, and P. A. Kollman. 1998. The early stage of folding of villin headpeace subdomain observed in a 200-nanosecond fully solvated molecular dynamics simulation. *Proc. Natl. Acad. Sci. U.S.A.* 95:9897–9902.

Eaton, W. A., E. R. Henry, and J. Hofrichter. 1991. Application of linear free energy relations to protein conformational changes: the quaternary structural change of hemoglobin. *Proc. Natl. Acad. Sci. U.S.A.* 88: 4472–4475.

El-Kettani, M. A. E.-C., and J. Durup. (1992). Theoretical determination of conformational paths in citrate synthase. *Biopolymers.* 32:561–574.

Elber, R., and M. Karplus. 1987. A method for determining reaction paths in large molecules: application to myoglobin. *Chem. Phys. Lett.* 139: 375–380.

Ferni, G., M. F. Perutz, B. Shaanan, and R. Fourme. 1984. The crystal structure of human deoxyhaemoglobin at 1.74 angstroms resolution. *J. Mol. Biol.* 175:159–174.

Fischer, S., and M. Karplus. 1992. Conjugate peak refinement: an algorithm for finding reaction paths and accurate transition states in systems with many degrees of freedom. *Chem. Phys. Lett.* 194:252–261.

Fujii, M., H. Hori, G. Miyazaki, H. Morimoto, and T. Yonetani. 1993. The porphyrin-iron hybrid hemoglobins. *J. Biol. Chem.* 268:15386–15393.

Gao, J., K. Kuczera, B. Tidor, and M. Karplus. 1989. Hidden thermodynamics of mutant proteins: a molecular dynamics analysis. *Science.* 244:1069–1072.

Geissler, P. L., and D. Chandler. 2000. Importance sampling and theory of nonequilibrium solvation dynamics in water. *J. Chem. Phys.* 113: 9759–9765.

Gelin, B. R., A. W. Lee, and M. Karplus. 1983. Hemoglobin tertiary structural change on ligand binding. Its role in the cooperative mechanism. *J. Mol. Biol.* 171:489–559.

Guilbert, C., D. Perahia, and L. Mouawad. 1995. A method to explore transition paths in macromolecules. Applications to hemoglobin and phosphoglycerate kinase. *Comp. Phys. Comm.* 91:263–273.

Harvey, S. C., and H. A. Gabb. 1993. Conformational transitions using molecular dynamics with minimum biasing. *Biopolymers.* 33: 1167–1172.

Henry, E. R., C. M. Jones, J. Hofrichter, and W. A. Eaton. 1997. Can a two-state MWC allosteric model explain hemoglobin kinetics? *Biochemistry.* 36:6511–6528.

Hofrichter, J., E. R. Henry, A. Szabo, L. P. Murray, A. Ansari, C. M. Jones, M. Coletta, G. Falcioni, M. Brunori, and W. A. Eaton. 1991. Dynamics of the quaternary conformational change in trout hemoglobin. *Biochemistry.* 30:6583–6598.

Huo, S., and J. E. Straub. 1997. The MaxFlux algorithm for calculating variationally optimized reaction paths for conformational transitions in many body systems at finite temperature. *J. Chem. Phys.* 107: 5000–5006.

Janin, J., and S. J. Wodak. 1985. Reaction pathway for the quaternary structure change in hemoglobin. *Biopolymers*, 24:509–526.

Janin, J., and S. J. Wodak. 1993. The quaternary structure of carbonmonoxy hemoglobin Ypsilanti. *Proteins.* 15:1–4.

Kavanaugh, J. S., J. A. Weydert, P. H. Rogers, and A. Arnone. 1997. High-resolution crystal structures of human hemoglobin with mutations at tryptophan 37$\beta$: structural basis for a high-affinity T-state. *Biochemistry.* 37:4358–4373.

Kiger, L., C. Poyart, and M. C. Marden. 1993. Oxygen and CO binding to triply NO and asymmetric NO/CO hemoglobin hybrids. *Biophys. J.* 65:1050–1058.

Kim, K. W., C. H. Lee, S. H. Jung, and Y. D. Won. 2001. Molecular dynamics simulations of a low oxygen affinity mutant hemoglobin. *Bull. Korean Chem. Soc.* 22:253–254.

Levy, A., V. S. Sharma, L. Zhang, and J. M. Rifkind. 1992. A new mode for heme–heme interactions in hemoglobin associated with distal perturbations. *Biophys. J.* 61:750–755.

Liddington, R., Z. Derewenda, E. Dodson, R. Hubbard, and G. Dodson. 1992. High resolution crystal structures and comparisons of T-state deoxyhaemoglobin and two liganded T-state haemoglobins: T($\alpha$-oxy)haemoglobin and T(met)haemoglobin. *J. Mol. Biol.* 228:551–579.

Luisi, B., B. Liddinton, G. Fermi, and N. Shibayama. 1990. Structure of deoxy-quaternary haemoglobin with liganded $\beta$ subunits. *J. Mol. Biol.* 214:7–14.

Luisi, B., and N. Shibayama. 1989. Structure of haemoglobin in the deoxy-quaternary state with ligand bound at the $\alpha$ haems. *J. Mol. Biol.* 206:723–736.

Mihailescu, M. R., C. Fronticelli, and I. M. Russu. 2001. Allosteric free energy changes at the $\alpha1\beta2$ interface of human hemoglobin probed by proton exchange of Trp $\beta$37. *Proteins.* 44:73–78.

Mihailescu, M. R. and I. M. Russu. 2001. A signature of the T→R transition in human hemoglobin. *Proc. Natl. Acad. Sci. U.S.A.* 98: 3773–3777.

Mouawad, L., and D. Perahia. 1996. Motions in hemoglobin studied by normal mode analysis and energy minimization: evidence for the existence of tertiary T-like, quaternary R-like intermediate structures. *J. Mol. Biol.* 258:393–410.

Mueser, T. C., P. H. Rogers, and A. Arnone. 2000. Interface sliding as illustrated by the multiple quaternary structures of liganded hemoglobin. *Biochemistry*, 39:15353–15364.

Murray, L. P., J. Hofrichter, E. R. Henry, M. Ikeda-Saito, K. Kitagishi, T. Yonetani, and W. A. Eaton. 1988. The effect of quaternary structure on the kinetics of conformational changes and nanosecond geminate rebinding of carbon monoxide to hemoglobin. *Proc. Natl. Acad. Sci. U.S.A.* 85:2151–2155.

Ogawa, S., and R. G. Shulman. 1972. High resolution nuclear magnetic resonance spectra of hemoglobin. III The half-ligated state and allosteric interactions. *J. Mol. Biol.* 70:315–336.

Olender, R., and R. Elber. 1996. Calculation of classical trajectories with a very large time step: formalism and numerical examples. *J. Chem. Phys.* 105:9299–9315.

Paoli, M., R. Liddington, J. Tame, A. Wilkinson, and G. Dodson. 1996. Crystal structure of T state haemoglobin with oxygen bound to all four haems. *J. Mol. Biol.* 256:775–792.

Perutz, M. F. 1970. Stereochemistry of cooperative effects in haemoglobin. *Nature.* 228:726–739.

Perutz, M. F., A. J. Wilkinson, M. Paoli, and G. G. Dodson. 1998. The stereochemical mechanism of the cooperative effects in hemoglobin revisited. *Ann. Rev. Biophys. Biomol. Struct.* 27:1–34.

Peterson, E. S., and J. M. Friedman. 1997. A possible allosteric communication pathway identified through a resonance Raman study of four $\beta$37 mutants of human hemoglobin A. *Biochemistry.* 37:4346–4357.

Ramadas, N., and J. M. Rifkind. 1999. Molecular dynamics of human methemoglobin: the transmission of conformational information between subunits in an $\alpha\beta$ dimer. *Biophys. J.* 76:1796– 1811.

Ryckaert, J.-P., G. Ciccotti, and H. J. C. Berendsen. 1977. Numerical integration of the Cartesian equations of motion for a system with constraints: molecular dynamics of n-alkanes. *J. Comp. Phys.* 23: 327–341.

Schlitter, J., M. Engels, and P. Kruger. 1994. Targeted molecular dynamics: a new approach for searching pathways of conformational transitions. *J. Mol. Graph.* 12:84–89.

Schumacher, M. A., M. M. Dixon, R. Kluger, R. T. Jones, and R. G. Brennan. 1995. Allosteric transition intermediates modelled by crosslinked haemoglobins. *Nature.* 375:84–87.

Shaanan, B. 1983. Structure of human oxyhaemoglobin at 2.1 Å resolution. *J. Mol. Biol.* 171:31– 59.

Shibayama, N., K. Imai, H. Morimoto, and S. Saigo. 1995a. Oxygen equilibrium properties of nickel(II)–iron(II) hybrid hemoglobins cross-linked between 82$\beta$1 and 82$\beta$2 lysyl residues by Bis(3,5-dibromosalicyl)fumarate: determination of the first two-step microscopic Adair constants for human hemoglobin. *Biochemistry.* 34: 4773–4780.

Shibayama, N., T. Yonetani, R. M. Regan, and Q. H. Gibson. 1995b. Mechanism of ligand binding to Ni(II)–Fe(II) hybrid hemoglobins. *Biochemistry.* 34:14658–14667.

Silva, M. M., P. H. Rogers, and A. Arnone. 1992. A third quaternary structure of human hemoglobin A at 1.7Å resolution. *J. Biol. Chem.* 267:17248–17256.

Smith, F. R., E. E. Lattman, and J. C. Carter, Jr. 1991. The mutation $\beta$99 Asp–Tyr stabilizes Y-a new, composite quaternary state of human hemoglobin. *Proteins.* 10:81–91.

Srinivasan, R., and G. D. Rose. 1994. The T-to-R transformation in hemoglobin: a reevaluation. *Proc. Natl. Acad. Sci. U.S.A.* 91: 11113–11117.

Tsai, C. H., T. Y. Fang, N. T. Ho, and C. Ho. 2000. Novel recombinant hemoglobin, rHb ($\beta$N108Q), with low oxygen affinity, high cooperativity, and stability against autoxidation. *Biochemistry.* 39:13719–13729.

Tsai, C.-H., T.-J. Shen, N. T. Ho, and C. Ho. 1999. Effects of substitutions of lysine and aspartic acid for asparagine at $\beta$108 and of tryptophan for valine at $\alpha$96 on the structural and functional properties of human normal adult hemoglobin: roles of $\alpha$1$\beta$1 and $\alpha$1$\beta$2 subunit interfaces in the cooperative oxygenation process. *Biochemistry.* 38:8751–8761.

Ulitsky, A., and R. Elber. 1990. A new technique to calculate steepest descent paths in flexible polyatomic systems. *J. Chem. Phys.* 92: 1510–1511.

Ulitsky, A., and D. Shalloway. 1997. Finding transition states using contangency curves. *J. Chem. Phys.* 106:10099–10104.

Unzai, S., R. Eich, N. Shibayama, J. Olson, and H. Morimoto. 1998. Rate constants for $O_2$ and CO binding to the $\alpha$ and $\beta$ subunits within the R and T states of human hemoglobin. *J. Biol. Chem.* 273:23150–23159.

Verlet, L. 1967. Computer "experiments" on classical fluids. I. Thermodynamical properties of Lennard–Jones molecules. *Phys. Rev.* 159: 98–103.

Waller, D. A., and R. C. Liddington. 1990. Refinement of a partially oxygenated T state haemoglobin at 1.5Å resolution. *Acta Crystallogr. Sect. B.* 46:409–418.

Zaloj, V., and R. Elber. 2000. Parallel computations of molecular dynamics trajectories using stochastic path approach. *Comp. Phys. Comm.* 128: 118–127.

Zhou, Y. X., Y. P. Feng, and Y. Takashi. 1991. Proton nuclear magnetic resonance and electron paramagnetic resonance investigation of alpha–alpha cross-linked Fe–Co hybrid hemoglobins. *J. Sci. China B.* 34:850–858.

Zuckerman, D. M., and T. B. Woolf. 1999. Dynamics reaction paths and rates through importance-sampled stochastic dynamics. *J. Chem. Phys.* 111:9475–9484.